NASA Contractor Report 3999

Incompressible Boundary-Layer Stability Analysis of LFC Experimental Data for Sub-Critical Mach Numbers

Scott A. Berry

COOPERATIVE AGREEMENT NCC1-24
JULY 1986

NASA

NASA Contractor Report 3999

Incompressible Boundary-Layer Stability Analysis of LFC Experimental Data for Sub-Critical Mach Numbers

Scott A. Berry

The George Washington University
Joint Institute for Advancement of Flight Sciences
Hampton, Virginia

Prepared for
Langley Research Center
under Cooperative Agreement NCC1-24

National Aeronautics
and Space Administration

**Scientific and Technical
Information Branch**

1986

ABSTRACT

An incompressible boundary-layer stability analysis of Laminar Flow Control (LFC) experimental data was completed and the results are presented. This analysis was undertaken for three reasons: to study laminar boundary-layer stability on a modern swept LFC airfoil; to calculate incompressible design limits of linear stability theory as applied to a modern airfoil at high subsonic speeds; and to verify the use of linear stability theory as a design tool. The experimental data were taken from the slotted LFC experiment recently completed in the NASA Langley 8-Ft. Transonic Pressure Tunnel. Linear stability theory was applied and the results were compared with transition data to arrive at correlated n-factors. Results of the analysis showed that for the configuration and cases studied, Tollmien-Schlichting (TS) amplification was the dominating disturbance influencing transition. For these cases, incompressible linear stability theory correlated with an n-factor for TS waves of approximately 10 at transition. The n-factor method correlated rather consistently to this value despite a number of non-ideal conditions which indicates the method is useful as a design tool for advanced laminar flow airfoils.

TABLE OF CONTENTS

LIST OF SYMBOLS

A	Disturbance amplitude
A_o	Initial disturbance amplitude
C_l	Coefficient of lift
C_p	Pressure coefficient
C_Q	Suction coefficient
$\tilde{C}_Q$	Integrated suction coefficient
f	Frequency, cps
M	Mach number
n	Logarithmic amplification ratio
q	Perturbation quantity
R	Reynolds number
RSL	Reference Suction Level (see appendix)
x,y,z	Spatial coordinates over wing surface where x is in the chordwise direction y is in the surface normal direction z is in the spanwise direction
U,V,W	Velocity components corresponding to coordinates x, y, z, respectively
x/c	Chord location
$2z/b$	Spanwise location
α	Wave number corresponding to x-direction
β	Wave number corresponding to z-direction
δ/c	Boundary-layer thickness
δ_f	Flap angle
λ/c	Wave length

Λ	Sweep angle, degrees
σ	Growth rate
ϕ	Amplitude function
ω	Circular frequency of oscillation, rad/sec

Subscripts

c	Chord
DES	Design condition
REF	Reference conditin
tr	Transition point
i	Imaginary component of complex function
∞	Free-stream conditions

Superscripts

$\sim$	Tranformed quantity in the direction normal to wave front

Other

NLF	Natural laminar flow
LFC	Laminar flow control
TS	Tollmien-Schlichting
CF	Crossflow
O-S	Orr-Sommerfeld
IF	Intermittency factor

LIST OF FIGURES

INTRODUCTION

Renewed interest in improving airplane performance characteristics has forced researchers to re-examine the possibility of achieving extensive regions of laminar flow on modern airplane wings. Aerodynamicists have long known that reduction in drag and an increase in performance would be realized if laminar flow were attained during cruising flight. The performance and feasibility of both natural laminar flow (NLF) and controlled laminar flow (LFC) airfoils were tested in the forties and sixties with mixed results. Though for some of these cases full-chord laminar flow was achieved, it could not be maintained at flight conditions representative of current modern transport designs. The construction techniques of the day did not produce a sufficiently smooth wing for laminar flow at flight Reynolds numbers. Furthermore, the poor off-design flight and stall characteristics were unimpressive. These results led to the dismissal of laminar flow as a viable drag reduction technique. However, recent advances in technology, along with a marked increase in fuel costs have sparked renewed research in laminar flow airfoils. New design methods as well as new construction materials and techniques have increased the viability of such concepts.

The design of laminar flow airfoils is dependent upon tools to model the boundary-layer characteristics correctly. Accurate prediction of the transition location is essential for determining the extent of laminar flow. Currently, the most reliable prediction technique is through the use of the e^n method, which is based on linear stability theory. The e^n, or n-factor, method is a semi-empirical technique which has gained credence from the fact that transition tends to correlate rather consistently with an n-factor value depending on the disturbance environment. For low disturbance tunnels,

n-factors of $n = 9$ corresponds fairly well to transition as established by Smith (ref. 1) and Van Ingen (ref. 2). For free flight, where turbulence levels are lower, transition seems to occur at much higher n-factors.[3,4] However, at present time there is only a limited amount of data available at flight conditions which are typical of high-performance transports. Validation of the use of the n-factor method for the higher Mach and Reynolds numbers of typical transport flight conditions is needed.

An experiment designed to examine supercritical LFC technology on a swept wing was conducted by NASA personnel in the Langley 8-Ft. Transonic Pressure Tunnel.[5] The overall objective of the experiment was to evaluate and document combined suction laminarization and supercritical airfoil technology at conditions which are typical of high-performance transports. Since linear stability theory was used in the design of this airfoil, an underlying goal of the experiment was to validate the use of this method as a design tool in the transonic regime. Therefore, the current thesis research, a stability analysis of the LFC experimental data, was conducted to correlate n-factors with transition at these high-performance transport flight conditions. The amplification of small disturbances for the swept LFC airfoil was calculated using the experimental pressure and suction data. Experimentally determined transition locations were compared with the results of these calcualtions and allowable amplification ratio limits were established. Measurements of the tunnel noise levels were made in order to assess the disturbance environment. The purpose of this thesis is to examine the disturbance growth problem in order to determine the design limitations of incompressible linear stability theory.

LINEAR STABILITY THEORY

Historical Development

The accurate prediction of transition is an important and formidable problem facing researchers today. A physically correct model of the transition phenomenon is, as yet, non-existent because of the complex nature of the problem. Currently, the most reliable method available is based on linear stability theory. Although this method has met with much success, it has received some criticism because of the limitations of the model itself. A discussion of these limitations follows in a later section. A brief history of the development of linear stability theory and its application as a transition prediction tool is given next. While a large number of scientists, mathematicians, and researchers have played an important role in the development, only a few of the more noted contributions will be discussed. This section is intended only to outline the more important steps in the development of a reliable transition predictor.

Much of the groundwork for the development of linear stability theory was laid down at or before the turn of the century. This early work on boundary-layer stability provided a strong foundation with which to develop the current transition prediction technique. The first examinations of consequence into the transition process were made separately by Helmholtz (1868), Kelvin (1871), and Rayleigh (1880). Their examination of the instability of inviscid flows provided some insights into the mechanisms of the transition phenomenon and also provided the initial theoretical formulation of the problem. Later, Reynolds (1883) performed his classic experiments on transition in a pipe. These experiments, which demonstrated the qualitative differences between laminar and turbulent flows,[6] provided the initial experimental investigation

into the problem of transition. An important breakthrough was made by Prandtl (1904) with his work on boundary-layer theory which allowed unification of experimental and theoretical work. Boundary-layer theory allowed experimental verification of the effects of viscosity. Prandtl (1921) also demonstrated the destabilizing effect of viscosity through the use of a simple linear model.[7] Previously, viscosity was thought to have a stabilizing influence.

The next important step in the development of linear stability theory was work done on the stability equation and two-dimensional disturbance waves. The theoretical understanding of the stability problem took a decisive turn when Orr (1907) and Sommerfeld (1908) separately developed the stability equation which became known as the Orr-Sommerfeld equation. Although they succeeded in setting up the equation, they were unable to generate the solution to the problem because of its complexity. It wasn't until various heuristic methods of approximation,[8] and later adequately developed asymptotic analysis methods, were used that solutions to the Orr-Sommerfeld equation were found. Work by Tollmien (1929), Schlichting (1935) and others was instrumental in this regard. Their work resulted in a highly-developed theory for the stability of the (two-dimensional) Blasius boundary layer.[7] Tollmien and Schlichting's model of transition remained experimentally unverified until the brilliant experimental work of Schubauer and Skramstead (1948) demonstrated the existence of instability waves in a boundary layer. Their work provided conclusive evidence that instability waves exist in a boundary layer with small external disturbances, and that Tollmien-Schlichting (TS) theory accounted for this behavior. More importantly, Schubauer and Skramstead showed that instability waves were a necessary precursor of transition.[7] These two-dimensional instability waves were found to travel

roughly in the direction of the free-stream flow and were subsequently referred to as Tollmien-Schlichting (TS) waves.

The need for wing sweep required extension of linear stability theory into three dimensions. It was Gray (1952) who first noticed that swept-wing boundary layers became turbulent much closer to the leading edge than straight-wing boundary layers.[9] Earlier, theoretical work in three dimensions had been simplified by Squire (1933) with a transformation that reduced the three-dimensional problem to an equivalent two-dimensional problem. This meant that two-dimensional solutions could be applied to three-dimensional flows. Experimental investigation of three-dimensional flows by Gregory, Stuart and Walker (1955) found in the boundary layer the existence of a set of vortices with their axes lying roughly in the direction of the local external stream. These vortices are referred to as cross-flow (CF) vortices. This confirmed the existence of a different mode or mechanism of transition when dealing with the three-dimensionality of swept wings. Flight tests were also important in exposing the mechanisms of boundary-layer instability due to swept wings. Pfenninger's (1958) work on swept wings with suction helped to provide an understanding of the basic problems of swept LFC boundary layers.

The underlying goal for the development of linear stability theory was to develop a consistent and reliable method for transition prediction. Previous methods for predicting transition proved unsuccessful until Smith (1956) and Van Ingen (1956) independently developed a semi-empirical method based on stability theory.[10] This, so-called, e^n or n-factor method has had a great deal of success in predicting transition and is currently the best known method of modeling the extent of laminar flow on an airfoil. Srokowski and

Orzag (1977) developed a user-oriented n-factor computer program called SALLY which stands for Stability Analysis, Local, Linear, Incompressible. This program solves the temporal O-S equation in order to find the amplification of disturbances within a boundary layer. Although this method ignores the influence of the initial disturbance environment, it has proved to be useful when calibrated against experimental data. A simplified code based on a table look-up method of finding the amplification of crossflow type disturbances was developed by Dagenhart (1981). Both codes have been shown to be adequate for indicating correct trends of the influence of various mean-profile modifiers upon transition,[11,13] thereby making them excellent design tools.

n-Factor Method

The n-factor method, which is based on linear stability theory has proven to be the most effective way of predicting transition at present. There are, of course, limitations to this method which are due to the assumptions implemented within linear-stability theory. An understanding of these limitations, and their possible implications on the results, is essential in order to properly apply the method and to get meaningful results. Therefore, a discussion of the relationship of linear stability theory and the n-factor method would be beneficial. First, a brief outline of the derivation of the stability equation, with emphasis on the important assumptions, will be presented. Then, discussion of the solutions of the stability equation as used in the n-factor method will follow. Finally, the assumptions of the stability theory will be examined in more detail in the hope of revealing its limitations. A more detailed explanation of the derivation of the stability equations can be found in texts by Betchov and Criminale (ref. 12), Rosenhead (ref. 9), and/or Dagenhart (ref. 13).

The derivation of the stability equation to be used in this analysis begins with the incompressible, three-dimensional, time-dependent Navier-Stokes equations. A perturbation assumption is first used to simplify these equations. The perturbation assumption reduces the flow within the boundary layer to a superposition of mean-flow and perturbation components. The mean flow term is assumed to be steady, parallel, and laminar. The resulting perturbation equations with the mean removed are then linearized by neglecting the quadratic terms in the perturbation quantities. Separating variables by assuming a complex form of the perturbation functions reduces these equations to ordinary differential form. This representation models the perturbations as travelling periodic disturbance waves that have a certain frequency and wavelength. These disturbances are allowed to amplify or damp in either space or time. The general form of perturbation function is

$$q(x, y, z, t) = \phi(y)\, e^{i(\alpha x + \beta z - \omega t)} \tag{1}$$

where $q(x, y, z, t)$ represents any of the perturbation quantities. A further simplification is introduced through the Squire transformation, which reduces the three-dimensional disturbance equation to a single quasi-two-dimensional disturbance equation in the direction of propagation of the wave front.[13] These transformations are

$$\tilde{\alpha}\,\tilde{x} = \alpha x + \beta z \tag{2a}$$

$$\tilde{\alpha}\,\tilde{U} = \alpha U + \beta W \tag{2b}$$

and

$$\tilde{\alpha}^2 = \alpha^2 + \beta^2. \tag{2c}$$

The angle between the direction of propagation of the disturbance wave front and the local inviscid flow at the edge of the boundary layer is defined as the wave angle. The mean velocity perpendicular to the wall is then neglected to obtain the Orr-Sommerfeld equation. This equation is the governing stability equation and can be used to model a two-dimensional travelling wave disturbance in a three-dimensional flow field. The Orr-Sommerfeld equation, given in reference 13, is listed here in its dimensionless form:

$$(\tilde{U} - \frac{\omega}{\tilde{\alpha}})(\phi'' - \tilde{\alpha}^2\phi) - \tilde{U}''\phi = -(i/\tilde{\alpha}R)(\phi'''' - 2\tilde{\alpha}^2\phi'' + \tilde{\alpha}^4\phi) \tag{3}$$

where ϕ is the disturbance amplitude as a function of the normal coordinate

$\tilde{U}$ is the steady-state velocity component in direction normal to disturbance wave front

$()'$ denotes differentation with respect to the normal coordinate

ω is circular frequency of oscillation

$\tilde{\alpha}$ is the wave number corresponding to the direction normal to the wave front and along the wing surface

R is the Reynolds number.

It can be shown that the amplitude of the disturbance $q(\tilde{x}, y, t)$ grows spatially as

$$A \sim e^{-\tilde{\alpha}_i \tilde{x}} \tag{4}$$

or

$$\frac{dA}{d\tilde{x}} = -\tilde{\alpha}_i e^{-\tilde{\alpha}_i \tilde{x}}. \tag{5}$$

The growth rate σ is defined as

$$\sigma \equiv \frac{1}{A}\frac{dA}{d\tilde{x}} = -\tilde{\alpha}_i \tag{6}$$

If the local growth rate is integrated from the initial point of amplification, total amplification can be found as

$$\int_{\tilde{x}_0}^{\tilde{x}} \sigma \, d\tilde{x} = \int_{\tilde{x}_0}^{\tilde{x}} \frac{1}{A}\frac{dA}{d\tilde{x}} \, d\tilde{x} = \ell n \frac{A}{A_0} \equiv n. \tag{7}$$

This defines the n-factor where n is the logarithm of the disturbance amplification from the neutral point. Using (6) in (7) yields

$$n(\tilde{x}) = -\int_{\tilde{x}_0}^{\tilde{x}} \tilde{\alpha}_i \, (\tilde{x}) \, d\tilde{x}. \tag{8}$$

Solutions to the stability (Orr-Sommerfeld) equation provide the necessary information for analyzing the growth of disturbances within the boundary layer. The Orr-Sommerfeld equation, along with the appropriate boundary conditions, constitutes a complex eigenvalue problem whose solution depends on the local mean flow field and the frequency, wavelength, and/or wave angle of interest. Two of the three variables (frequency, wavelength, or wave angle) may be specified with the third given by the solution of the O-S equation. For these given conditions, a local disturbance growth rate can be found. Integrating the local growth rate, as in eq. 8, from the initial point of amplification (neutral point) gives the logarithm of the total amplification. The total amplification within the boundary layer is used as an indicator of transition. This is the basis of Smith and Van Ingen's n-

factor method where n is a running integral of the local amplification rate from the neutral point. The n-factor method is based on the fact that at a given value of n, transition is likely to occur. Previous studies have indicated that correlation of the n-factor method with low-disturbance wind tunnel transition data occurs around a value on the order of ten.[1,2,10,11]

Several assumptions were used in the derivation of the Orr-Sommerfeld equation: (1) flow is incompressible, (2) flow is parallel, (3) nonlinear terms can be neglected, and (4) mean flow perpendicular to the wall can be neglected. A discussion of the effect of each assumption on the solution follows. The first assumption, that of incompressible flow, means that the density fluctuations are neglected. This, of course, is appropriate at low Mach numbers where the effect of compressibility is very small, but at the Mach numbers of the present analysis, compressibility effects should be considered. However, studies by Mack (ref. 19) and others have shown that the use of incompressible codes overpredict the local amplification rates for Mach numbers in the present range. Thus, compressibility has a stabilizing influence so that the use of an incompressible stability code should overpredict the disturbance amplification (a "conservative" approach). The second assumption used is that the boundary-layer mean flow is parallel. According to Schlichting (ref. 14) parallel flow is a good approximation of boundary-layer flow since the dependence of the velocity u on the y-coordinate is at least an order of magnitude greater than that on x. For the present analysis, the boundary layer is altered by suction through closely spaced slots. Distributed, or continuous, suction tends to make the boundary layer more nearly parallel after the initial growth in thickness near the leading edge. On the other hand, discrete suction (through slots) could cause local

"dimpling" of the streamlines which is counter to the parallel flow assumption. However, the effect of this streamline distortion should be small. Thus the parallel flow assumption is fairly good. The next assumption, linearization, means that the quadratic terms within the governing equations are neglected. Strictly speaking, this is justified only for infinitesmally small disturbances. In reality, the perturbation amplitudes are not infinitesmally small, but small enough such that the amplification process can be considered essentially linear. It is assumed that the linear amplification of disturbances dominates the process leading to transition and that nonlinear interaction and breakdown is reserved for a relatively short period just prior to transition. Thus, correlation of the n-factor method with transition data should be made at the beginning of transition (i.e., first appearance of turbulent bursts). The fourth assumption, that the normal velocity component is zero, seems contradictory to the fact that there is suction. However, as noted by Dagenhart (ref. 13), the most important effect of suction is modification of the streamwise mean flow velocity profile and its derivatives. Therefore, the impact of suction is manifested through the streamwise velocity terms retained in the Orr-Sommerfeld equation, and the error in neglecting the normal velocity component should be small.

The theory as used in this research has been shown to be in reasonable agreement with experimental data.[13] There are discrepancies between theory and experiment, however, which can be attributed to these various assumptions. Independent work, such as Malik's work on compressibility and Saric and Nayfeh's work on non-parallel effects, is continuing in order to reintroduce these assumptions into the theory. Criticisms of linear stability theory, however, arises not from the use of these assumptions but from the

inability of the general theory to properly model the complete transition process. The mechanisms of transition can be thought of as occuring in three phases: (1) introduction of small disturbances into the boundary layer; (2) subsequent amplification of these disturbances by linear processes within the boundary layer; and (3) nonlinear breakdown to turbulence. The n-factor method and linear stability theory do a good job of modeling the second phase of transition, the linear amplification of small disturbances. The third phase, the nonlinear breakdown, is, of course, beyond the capabilities of a linear theory. However, if the beginning of transition is used as the correlation point, and if the interaction of streamwise and crossflow type disturbances are kept to a minimum, then this should not be important. The first phase, the introduction of small disturbances into the boundary layer (Morkovin's receptivity problem), on the other hand, is unaccounted for by linear stability theory. The influence of the external disturbance environment on boundary-layer stability remains an unknown.

The disturbance environment appears to play an important role in determining transition n-factors. Studies by Pfenninger, Bacon, and Carlson (refs. 28-31) and Spangler and Wells (ref. 24) have shown the importance of the effect of acoustical noise on the stability of laminar boundary layers. These reports suggest that the spectral energy distribution near the critical band of amplified frequencies, and not the overall energy levels, is the more important influence upon transition. The relationship between transition and free-stream disturbance spectra, however, is not fully known at this time.

Boundary-Layer Instabilities

Boundary-layer transition is a fluid dynamic phenomenon which has received a great deal of attention since the turn of the century. The conceptual model of this problem is still relatively in its infancy. However, this much is known: that transition to turbulence can be caused by instability waves in the boundary layer. Modern airfoils are faced with a number of instabilities which can reduce the extent of laminar flow over the surface. Amplification of disturbances by Tollmien-Schlichting, crossflow, or Görtler mechanisms over a certain threshold will cause premature transition. In order to maximize the extent of laminar flow, each, and subsequently any combination (the interaction problem) of these instabilities must be avoided or at the very least minimized. Of these, the TS and CF type disturbances are most commonly considered in modern airfoil design and analysis problems. Fortunately, computer codes designed to model these two disturbance types are available. Furthermore, correlation of these codes with experimental data is required to validate them as design tools. It is for these reasons that the TS and CF type disturbances are examined in the present analysis.

Modern wings designed for transonic flight are generally swept. Figure 1 shows a typical swept-back wing planform with its curved streamlines. Very near the surface, the boundary-layer streamline will have a curvature that is more pronounced than the potential flow streamline, which sets up a three-dimensional velocity field in the boundary layer. This three-dimensional field can be broken up into a streamwise component, parallel to the local potential streamline, and a crossflow component, perpendicular to the local potential streamline. Figure 2 shows the streamwise and crossflow components of a typical swept wing boundary-layer profile. Note that there is an

inflection point in the crossflow profile which is due to the imposed boundary conditions of no slip at the wall and the asymptotic approach to zero velocity at the boundary-layer edge. Rayliegh, as noted earlier, has shown that velocity profiles with inflection points are dynamically highly unstable even in the absence of viscosity. Thus, associated with the crossflow velocity component is an instability which is inviscid in nature and is due primarily to the existence of an inflection point in the velocity profile. This instability is referred to as crossflow (CF) instability. Velocity profiles without inflection points, for example the Blasius boundary layer, were initially thought to be inherently stable. Prandtl first noticed the mildly destabilizing effects of viscosity. Tollmien and Schlichting examined this type of profile in detail with the OS equation (which includes viscous effects) and also found viscosity to be destabilizing. Thus, the instability which arises from viscous effects was originally referred to as Tollmien-Schlichting (TS) instability. However, for flow with non-zero pressure gradients (for instance our swept-wing case), inflection points can develop in the streamwise profile which is further destabilizing. An adverse or positive pressure gradient promotes highly destabilizing inflection points in the streamwise profile. Therefore the instability associated with the streamwise component can be due to either viscous effects or inflection points in the profile.

Dagenhart, reference 13, discussed the fact that there are two wave angle orientations that maximize the disturbance amplification rates. These orientations correspond roughly with the streamwise and crossflow velocity directions. Squire has shown that for incompressible flow, the TS disturbances which amplify the most are those moving in the direction of the

free-stream flow. For this reason, the constraint of a wave angle of zero is applied to the TS stability calculations which follow. Gregory, Stuart and Walker (ref. 15) and Pfenninger (ref. 16) have shown by flow visualization techniques that CF vortices align approximately in the potential flow direction and are stationary. Furthermore, calculations by Srokowski and Orzag (ref. 17) indicate that these stationary disturbances are usually the most highly amplified. Therefore, a frequency of zero is assumed for the CF stability calculations which follow.

Suction thins the boundary layer and modifies the profile shape.[17] Figure 3 qualitatively illustrates the effect of suction on both the streamwise and crossflow profiles. In the case of the streamwise profile, suction draws the velocity profile down and tends to remove any inflection points. This greatly improves the stability of the streamwise flow. For the crossflow profile, however, suction is not as effective. As noted by Brown (ref. 18) and Mack (ref. 19), suction is more efficient at controlling TS instabilities than CF instabilities. The crossflow profile must have an inflection point because of the boundary conditions. Therefore, suction can only draw the inflection point down where viscous effects can influence and slow the disturbance growth rates.

Computer Codes

The incompressible stability characteristics of laminar compressible boundary layers on swept, tapered wings with suction are calculated by an Orr-Sommerfeld equation solver. This computational method can model both the TS and CF type disturbances within the boundary layer. In the analysis mode, two separate codes are required: one to calculate the boundary-layer velocity profiles, and one to calculate the stability characteristics. The boundary-

layer velocity profiles were obtained from a program written by Kaups and Cebeci (ref. 20) (referred to as the CEBECI code) while the stability characteristics were found using either the SALLY code of Srokowski and Orzag (ref. 17) or the MARIA code written by Dagenhart (ref. 13).

The CEBECI code calculates the compressible three-dimensional velocity profiles of a laminar boundary layer on a swept and tapered wing with suction. An efficient two-point finite-difference method is used to solve the boundary-layer equations. Input to the program includes the streamwise pressure and suction distributions, free-stream flow conditions and wing geometry information. Upper and lower surface boundary layers are calculated separately. Program output which includes both the spanwise and streamwise components of the velocity distribution is saved in magnetic disk files in formats appropriate for both SALLY and MARIA codes.

The SALLY code models the amplification of a travelling wave type disturbance from the initial point of amplification in a laminar boundary layer. The code utilizes Chebyshev polynomials to approximate solutions to the Orr-Sommerfeld equation. Input includes the boundary-layer velocity profiles from the CEBECI analysis along with the particular wavelength, frequency and/or wave angle of interest. Two of the three variables (wavelength, frequency and wave angle) may be specified while the third is part of the solution along with the amplification rate. Separate computer runs are required to model either the TS or CF type disturbances. For analysis of TS disturbances, the wave angle is fixed at zero (for 2-D waves) and the frequency range is specified. For analysis of CF disturbances, the frequency is fixed at zero (for standing waves) and the range of wavelengths is specified. Output is the natural logarithm of the growth of the

disturbance from the initial point of instability along the airfoil. It should be noted, however, that due to an inadequacy of the solution technique utilized within SALLY, the code is unable to calculate disturbance damping. This is due to the technique's ability to trace only eigenvalue solutions which predict amplification.

The MARIA code approximates the amplification of the CF type disturbance only. A table look-up method based on stability charts generated by SALLY is used. This code has been shown (ref. 13) to adequately model the CF instability for preliminary and trade-off analyses and, if needed, shows the critical wavelengths for a more accurate SALLY run. The use of this code initially should reduce the overall computer time and costs.

LAMINAR FLOW CONTROL EXPERIMENT

Design and Set-Up

An experiment designed to evaluate the compatibility of laminar flow control and advanced supercritical airfoil concepts has been conducted recently by NASA in the Langley 8-Ft. Transonic Pressure Tunnel. This experiment examined the possibility of reducing friction drag through laminarization with local suction at simulated flight conditions which are representative of future transport designs. A large chord, swept supercritical airfoil with suction was tested over a wide range of flight conditions up to and within the transonic regime, which includes the design point case of M_∞= 0.82 and R_C = 20 million. A detailed discussion of the test design and setup was presented by Harvey and Pride (ref. 5). This LFC experimental concept was designed using the latest analytical methods. One of the major objectives of the experiment therefore was to validate these design techniques. The present results will not include the experimental design point data due to a classification restriction on this information. However, the off-design test points will allow adequate examination of the disturbance growth problem.

The experimental setup, as shown in figure 4, consists of the swept-wing model and the contoured liner, both of which were designed for tunnel conditions of M_∞ = 0.82 and R_C = 20 million and sweep angle $\Lambda = 23^0$. The aerodynamic design considerations of the swept LFC wing were discussed in papers by Pfenninger, Reed and Dagenhart (ref. 21) and Allison and Dagenhart (ref. 22). The wing was designed to examine suction laminarization at conditions which simulate full-scale flight conditions. The design considerations of the contoured tunnel liner were discussed in a paper by

Newman, Anderson and Peterson (ref. 23). The contoured liner installed on all four walls of the test section is intended to simulate interference-free flow about an infinite-span, yawed wing at the design test condition. This is a point design for a highly sensitive transonic condition, therefore, contoured liner performance is expected to be degraded at off-design conditions. The effect of off-design testing will be discussed later. In order to approach free-flight disturbance levels within the test section, a combination of honeycomb, screens and choke-plates were installed in the tunnel.

Measured Data

Instrumentation for the LFC experiment includes pressure orifices, suction metering system, surface thin-film sensors for locating transition and acoustic transducers for measuring dynamic pressure data. These instruments provide the necessary information to correlate the n-factor method. The primary test surface of the LFC experiment is the upper surface, therefore, the present results are based on the upper surface data only. A sketch of the upper surface instrumentation is shown in figure 5. The pressure distribution along the densely-packed center-line row of orifices, plus the suction distribution are the basic input into the stability analysis in order to calculate the growth of disturbances within the boundary layer. This growth is then compared with the transition data in order to arrive at a transition n-factor. This is the basic method of correlation to be used in this paper.

Figure 5 is a sketch illustrating both chordwise and spanwise rows of pressure orifices. This array of orifices provides the means for measuring the three-dimensional flow field about the upper surface of this airfoil. The flow field is expected to be non-uniform since the cases to be analyzed (M_∞ = 0.4, 0.6, 0.7) are at off-design Mach numbers. Shown in figure

6 for the center span are experimental chordwise pressure distributions (symbols) for all three Mach numbers against the theoretical design point pressure distribution (dashed line). This figure reveals that the experimental pressure distribution differs considerably from design for all three Mach numbers in the following regions: (1) $0.2 \lesssim x/c \lesssim 0.20$ (a steep adverse pressure gradient), and (2) $0.20 \lesssim x/c \lesssim 0.80$ (a slightly favorable pressure gradient). In the region where there is an adverse gradient, disturbance amplification is expected, while damping is likely for a region with a favorable gradient. Since the pressure distribution is scaled by the free-stream dynamic pressure, the three C_p plots appear similar. Close inspection, however, shows that the pressure peak rises slightly with increasing Mach number. Also, as can be seen in figure 6, these three Mach numbers are all subcritical. Inspection of the spanwise pressure distributions shown in figure 7 shows that a gradient exists along lines of designed constant pressure. These design isobars coincide with the suction slots running along lines of constant percentage of chord. The spanwise gradient effect is more pronounced at the leading and trailing edges. The fact that the pressure distribution changes with spanwise location suggests that as the suction levels are changed the transition pattern will move non-uniformly. This phenomenon will be seen in the transition data to be presented later. This spanwise gradient is an indication that the liner performance is degraded at these off-design Mach numbers.

Suction air is removed through closely spaced fine slots extending spanwise along constant percentage of chord. Details of the suction system design are given in reference 5. Evaluation of the suction rates required to avoid premature transition on the swept LFC airfoil was based on incompressible

stability analysis at the design condition. Since non-ideal pressure distributions are being analyzed, the optimum suction distribution required for laminarization differs from the design suction. This is shown in figure 8, where two theoretical suction distributions, one for the design case and one for an off-design case, are plotted with two experimental suction distributions. It can be seen that the experimental suction levels are quite a bit higher than the theoretical levels. The experimental suction distributions required to maintain full-chord laminar flow are higher because the Mach numbers are off-design.

Suction levels required to maintain laminar flow are greatly influenced by Reynolds number. A parameter, which is referred to as Reference Suction Level (RSL), was defined in order to remove this Reynolds number dependence. The RSL parameter is defined as

$$RSL = \tilde{C}_Q / \hat{C}_{Q_{REF}}$$

where $$\tilde{C}_Q = \int_0^1 C_Q(x/c)d(x/c)$$

and $$\hat{C}_{Q_{REF}} = \sqrt{R_{c_{DES}}/R_c} \int_0^1 C_{Q_{DES}}(x/c)d(x/c).$$

A detailed discussion of the development of this parameter is in the Appendix. The RSL coefficient is the actual integrated suction level scaled by a reference integrated suction level which is based on Reynolds number. This essentially allows suction parameter comparisons based on removal of equal fractions of the boundary layer.

Throughout the experiment, the suction distribution maintained the same

basic shape as the design distribution-only the overall levels were changed. This allows the RSL parameter to be an indication of the effect of overall suction on boundary-layer instabilities. Experimental data were taken by setting the desired Mach and Reynolds number combination in the test section with overall suction at its maximum level and then examining the transition pattern as the overall level was reduced. This provided several test cases for a range of suction levels at each Mach and Reynolds number. This is referred to as a suction excursion. As will be discussed later, the suction excursion is essential in order to arrive at transition n-factors. Thus, a RSL parameter variation, which represents a suction excursion, will be the primary method used to examine the dependence of boundary-layer stability on suction levels.

Hot-film sensors deposited on one end of a tiny quartz rod were mounted flush with the surface at locations shown in figure 5. The sensors were controlled by a constant temperature anemometer at 80°C above local recovery temperature. The installation technique for the hot-film sensors on this model is given in reference 5. The hot-film sensors were used to analyze the local boundary-layer state. There were a total of 25 sensors distributed on the upper surface: 9 along the mid-chord line, with the remainder positioned in a dense array in the aft pressure recovery region. This arrangement was chosen to provide detailed coverage of the changing transition pattern at the design condition, which was expected to move in a two-dimensional fashion. For off-design conditions, however, the transition pattern moved non-uniformly. Therefore the distribution of sensors shown was not as thorough as was desirable. The effect of this will be discussed later. Examples of some voltage traces, their corresponding boundary-layer states and their locations

on the upper surface are shown in figure 9. The transition pattern shown is typical of the data analyzed. The amplitude of the fluctuating value of the sensor voltages indicates the relative condition of the boundary layer. The low amplitude dynamic signal indicates the lower shear stress that is representative of a laminar boundary layer and is typically found as shown in the figure. The higher amplitude dynamic signal indicates the higher shear stress that represents a turbulent boundary layer. The transitional type boundary layer has both the laminar and turbulent type signals and it is the relative amount of each, or intermittency factor (IF), which indicates the fraction of time that the flow is turbulent. For example, a signal that shows turbulent flow of 80 percent of the time has an IF of 8.

A major component of a complete stability analysis, as noted in recent studies by Spangler and Wells (ref. 24) and Mack (ref. 25), is an understanding of the disturbance environment influencing transition. Mack notes in reference 25 that any empirical transition criteria can only be valid for a specific disturbance environment. Therefore, measurements of the dynamic pressure data were taken in order to assess the specific disturbance spectral levels that were present in the test section for different test conditions. Acoustic transducers, which are Hemholtz-cavity mounted within cylindrical elliptic-nose probes, were used to measure the fluctuating pressures. The probes were mounted on a strut located upstream of the wing leading edge in order to measure the free-stream disturbance levels impinging on the model. Dynamic signals were recorded on a tape recorder, and were later analyzed using a high resolution digital spectrum analyzer. The transducer signals were corrected for electronic noise using a technique outlined in reference 26. A sample energy spectrum is shown in figure 10 with electronic noise

subtracted out of the raw data and then converted to obtain the corrected disturbance spectrum.

STABILITY ANALYSIS

The upper surface LFC experimental boundary layer was analyzed for TS and CF disturbances. Only the off-design results are presented. The TS analysis was completed using the SALLY code, while the CF analysis was completed using the MARIA code. A total of 90 separate data cases were analyzed in which the 3 main parameters (RSL, M_∞ and R_C) were varied. To show representative n-factor calculations, one set of data cases was chosen in which the suction parameter was varied while the Mach and Reynolds numbers were held constant. This set was chosen to illustrate how the transitional n-factors were inferred from the analyzed data. Summary plots will follow in which the results of all the cases are presented. Attached laminar flow up to the experimentally determined transition location was computed for all cases considered.

Suction Excursion

As stated before, the transition pattern moves non-uniformly spanwise as the overall suction level is changed for the off-design Mach number cases being analyzed. The reason for this is that the tunnel liner is mis-matched for its intended purpose at these Mach numbers. The liner was intended to provide infinite swept flow (the chordwise pressure distribution should remain constant along the span) at the design condition. Since the off-design conditions are being analyzed, the liner does not correctly divert the flow in an infinite swept fashion. Therefore, the transition pattern moves three-dimensionally. Figure 11 shows that as the suction levels are reduced for constant M_∞ and R_C, as indicated by a reduction in RSL, the transition pattern sweeps down towards the center-span row of orifices. At some point, when the suction level is reduced far enough, the line corresponding to the beginning of transition jumps forward at mid-span. Along the center row of orifices,

the transition pattern almost instantaneously changes from 100 percent chord laminar to nearly 100 percent chord turbulent. Because of this phenomenon, a different method of correlating n-factors with transition was used for this analysis. In previous methods, the transition n-factor was found by calculating an n-factor corresponding to the experimentally determined transition point. For the present method, transition n-factors were found by locating the maximum calculated n-factor in the nose region at the moment transition moves forward of the initial thin-film gage. Thus, it takes a suction excursion of points to estimate the correct n-factor corresponding to transition at each Mach and Reynolds number combination.

Sample Cases

Inferred transitional n-factors were arrived at by examining suction excursions at each Mach and Reynolds number combination. To illustrate the basic correlation method, a representative excursion will be discussed in some detail. The cases that follow represent a suction excursion at $M_\infty = 0.6$ and $R_C = 10 \times 10^6$. Figures 12 thru 15 present the results of the SALLY and MARIA calculations for each of the 4 cases. Shown on the plots are the calculated logarithmic amplification ratios for a range of frequencies or wavelengths and the pressure and suction distributions along the chord. For the curves showing the TS instability, the dotted lines represent the area of neutral stability or damping and the symbols correspond to the frequencies listed in the table. For the CF curves, only the most critical wavelength and corresponding maximum n-factors are listed.

Case 1

The TS and CF stability calculations for a suction parameter RSL = 1.8 are shown in figure 12. The corresponding transition location along the

center station, as shown in figure 11, is $(x/c)_{tr} > 95$ percent. Figure 12a shows that for TS growth, the most amplified frequency is f = 14 kHz which reaches a logarithmic amplification ratio of n = 7.413 in the nose region, followed by a mid-chord stable or damped region and a subsequent growth near the trailing edge. The growth that is calculated near the tail occurs past the last suction slot and is beyond all thin-film instrumentation. Furthermore, since the mid-chord region, in which no amplification is predicted, is large and since SALLY is unable to predict damping, the actual disturbance amplitudes near the trailing edge should be much lower. For these reasons the growth near the tail is ignored. As stated in figure 12b, CF disturbances only experience an integrated logarithmic amplification of n = 0.72 in the nose region for the critical wavelength $\lambda/c = 0.0006$, followed by a stable region to the tail. Obviously, TS amplification is the dominant instability. Furthermore, a TS growth of n = 7.4 at the nose did not force transition to occur anywhere along the chord.

Case 2

The stability calculations for a suction parameter RSL = 1.37, with a corresponding full-chord laminar flow, are shown in figure 13. For TS growth, figure 13a shows that for the most amplified frequency f = 14 kHz, a logarithmic amplification ratio of n = 9.0 is reached in the nose region, followed by a mid-chord damped zone and then a subsequent growth near the tail. Again, the growth in the tail region is overpredicted and is ignored. As depicted in figure 13b, the maximum amplification ratio for CF instability is n = 0.78 for a critical wavelength $\lambda/c = 0.0006$ and this occurs in the nose region. TS amplification is still the dominant instability and a growth of n = 9.0 in the nose region still did not produce early transition.

Case 3

Figure 14 shows the stability calculations for a suction parameter RSL = 1.25. As can be seen in figure 11, the transition location along the center span has moved forward slightly to $(X/C)_{tr} \approx 85$ percent. Figure 14a shows that for TS growth, the most amplified frequency is f = 11 kHz which reaches a logarithmic amplification ratio of n = 9.84 in the nose region, followed by a mid-chord stable region all the way back to transition. For CF instability, a maximum amplification ratio of n = 0.76 is reached at the nose for a critical wavelength of $\lambda/c = 0.0006$ as stated in figure 14b. The CF growth is still relatively insignificant. However, a TS growth of n = 9.84 in the nose region corresponds to a 15 percent forward shift in the transition location.

Case 4

The TS and CF stability calculations for a suction parameter RSL = 1.15 are shown in figure 15. The transition location corresponding to this case, as shown in figure 11, has moved forward of the initial thin-film gage. Therefore transition has occurred fairly close to the leading edge. Figure 15a shows that for TS growth near the leading edge, the most amplified frequency is f = 12 kHz which reaches a logarithmic amplification of n = 10.52 before becoming stable. Figure 15b depicts that for CF growth near the leading edge, the most amplified wavelength is $\lambda/c = 0.0006$ which reaches a logarithmic amplification ratio of n = 0.77. TS amplification remains the dominant instability. More importantly, a TS growth near the nose of n = 10.52 corresponded with transition occurring near the leading edge.

Data Summary

Stability analyses of off-design LFC experimental data, over a range of Mach numbers, Reynolds numbers, and suction levels, was completed and the

results are tabulated in table 1. TS instability was found to dominate the process leading to transition while CF growth was small enough such that interaction of these two disturbances seems unlikely. A summary of the TS amplification for all cases considered is presented in figures 16, 17 and 18. Each figure corresponds to one Mach number in which the calculated TS logarithmic amplification ratios (n_{TS}) are plotted against Reynolds number (R_c) for a number of suction levels (RSL). The symbols represent the condition of the flow - open symbols for full-chord laminar flow, closed symbols for full-chord turbulent and half-open symbols for transition occuring along the chord between the most-forward and most-rearward thin-film gages. These plots are used to indicate at what level of TS amplification transition is likely to occur. The dashed lines that are sketched in indicate the n-factor limits corresponding to transition. The symbols with flags signify a phenomenon, referred to as oversuction, that was observed in the transition data. This phenomenon shall be discussed in more detail later. The three data sets corresponding to each Mach number were not as complete as was desirable. At the lowest Mach number, the range of suction test cases available for analysis did not provide a sufficient band of n-factors at transition. Therefore, the figures will be discussed in descending order of completeness.

A phenomenon was observed in the transition data for the cases with the combination of high suction levels, and high Mach and Reynolds numbers. This phenomenon amounted to a reduction in the laminar zone at the highest suction levels which disappeared as the suction levels were reduced. Shown in figure 19 is an example of the transition data which demonstrates this phenomenon. The figure depicts transition patterns for cases with a range in suction level

(RSL) at M_∞ = 0.6 and R_c = 18 million. The lines shown on the upper surface plot represent the beginning of transition for each case as revealed by the hot-film sensors. At the highest suction levels (RSL = 2.56) transition occurs as far back as 100 percent on either side of mid-chord, but along the mid-chord line transition is at about 85 percent chord. As RSL is reduced to 2.16, the transition line moves towards the tail and is at $(x/c)_{tr} \approx 90$ percent along the mid-chord. For RSL = 2.01 transition at the mid-chord line has moved back beyond the last hot-film sensor, but the transition line has moved forward for the outboard region at the top of the figure. As the suction is reduced even further, transition again jumps forward as discussed earlier and as shown in figure 19. It seems that this loss of laminar flow at high suction levels may be due to sensitivity to surface roughness. Inspection of figure 5 which shows the instrumentation (pressure orifices, hot-film and acoustic sensors) suggests that the maximum roughness due to instrumentation occurs along the centerline of the model. Too much suction will excessively thin the boundary layer, such that transition is governed by surface roughness and not by disturbance amplification. These cases that demonstrate such behavior are referred to as oversuction cases and are shown in figures 16, 17, and 18 as half-open symbols with a flag.

The most complete data set is at M_∞ = 0.6. The data shown in figure 17 clearly define the transitional limits. Suction levels which allow TS amplification factors greater than $n \approx 10$ at the lower Reynolds numbers to $n \approx 11$ at the higher Reynolds numbers are insufficient to maintain laminar flow. On the other hand, suction levels which allow up to $n \approx 9$ at the lower Reynolds to $n \approx 10$ at the higher Reynolds numbers should maintain full-chord laminar flow. The effect of surface roughness can be seen in the figure,

where at the higher Mach and Reynolds numbers, suction must be reduced to attain full-chord laminar flow. To summarize at $M_\infty = 0.6$, logarithmic amplification of TS type disturbances with $n > 10$ leads to transition.

The next best data set is at $M_\infty = 0.7$. Figure 18 shows that the data available indicate the allowable n-factor range at transition. A TS logarithmic amplification of $n \approx 10$ is allowable without reduction in full-chord laminar flow. However, TS amplification ratios of $n > 10.5$ for the low Reynolds numbers to $n > 11$ for the high Reynolds numbers indicates that transition will occur far forward on the model (essentially full-chord turbulent flow). The correlation trends for this set of data is in close agreement with the data at $M_\infty = 0.6$. However, the effect of surface roughness appears to be more critical at $M_\infty = 0.7$. This can be seen in figure 18 where the flagged data cases are encroaching on the transition limit, to the point where full-chord laminar flow may be difficult to attain at any suction level for the higher Reynolds numbers. Excessive boundary-layer thinning may be a problem which warrants further study at the higher Mach and Reynolds numbers.

The last data set is for $M_\infty = 0.4$ and is shown in figure 16. Because, at this Mach number, it was difficult to get transition along the center span even at the minimum attainable suction levels, the data seem inconclusive. However, based on the results at the other two Mach numbers and some engineering judgment, transition limit lines can be sketched in as shown. If this speculation is correct, then a TS logarithmic amplification of $n \approx 8.5$ at the low R_C to $n \approx 9$ at the high R_C would correlate with transition. This trend is in agreement with the higher Mach numbers, even though the levels are a bit lower. For this Mach number, surface roughness effects appear in the

transition data only at the highest Reynolds number, R_c = 20 million.

Discussion of Results

The off-design conditions induced spanwise pressure gradients and large minimum pressure peaks near the nose of the airfoil. This produced spanwise variations in boundary-layer development, disturbance amplification near the leading edge and a large stable TS zone. Three-dimensional pressure and transition patterns developed which caused the abrupt jump of transition to the leading edge as the suction level was reduced. All these factors contributed in increasing the difficulty of correlating n-factors at transition. However, despite the non-ideal conditions, the calculated n-factors at transition are in reasonable agreement with previous studies.

The TS disturbances were amplified only over a small region near the leading edge due to a combination of factors. First, sharp minimum pressure peaks were generated near the leading edge because the Mach numbers considered were less than the design Mach number. This creates a negative pressure gradient, which is greatly destablizing for TS disturbances, and therefore, a region where, in the absence of suction, strong disturbance growths could be expected. As stated before, TS disturbances are greatly stabilized by suction. Secondly, the suction distribution and, more importantly, the suction system (slot geometry, spacing and locations) were designed for a free-stream Mach number of 0.82 and Reynolds number of 20 million. The initial suction slot is located at approximately 2.5 percent chord which is slightly aft of the pressure peak. In general, TS disturbances have begun to amplify before the initial suction slot. Suction should, ideally, be applied just prior to and over a region of disturbance growth. Thus, in the sense that amplification is allowed to take place without suction being applied,

this present suction system is not ideal for handling the off-design Mach numbers. The analysis also shows that, once suction is applied, TS disturbances are damped very quickly and remain stable past the last suction slot. The entire amplified band of frequencies is stabilized, for all suction levels, roughly 2.5 percent chord after the initial suction slot. This implies that if suction were available closer to the leading edge and just prior to the pressure peak, then the calculated growth rates for these off-design cases would be less severe. Thus, full-chord laminar flow could be maintained for both lower values of suction and higher chord Reynolds numbers at each Mach number.

The calculated logarithmic amplification ratios at transition change with Mach number, as depicted in figure 20. Both TS and CF n-factors at transition are shown for the range of Reynolds numbers analyzed. Based on the figure, one can see that TS amplification is the dominant instability. CF amplification is relatively small and does not appear to be a problem until the Mach number approaches the design value. Curiously, the TS transitional n-factors are increasing slightly with Mach number. Examination of the noise levels, in terms of measured pressure fluctuations (in percent of local free-stream conditions), for the 8-Foot Transonic Pressure Tunnel shown in figure 21 (taken from ref. 27), shows that acoustic noise levels increase with Mach number. One might expect that based on this, the transition n-factors would decrease with Mach number. Since the opposite happens, perhaps the overall noise levels are relatively unimportant. Figure 22 shows the disturbance frequency spectra for the Mach numbers in question. These sample curves, taken from the acoustic data measured upstream, show that the overall noise level, represented by the area under each curve, increases with Mach number.

However, in the range of frequencies critical for TS amplification ($10 < f < 20$ kHz), the curve for $M_\infty = 0.4$ has peak fluctuations higher than that at the other two Mach numbers. Therefore, it appears that the disturbance amplitudes within the critical band of amplified frequencies is more important than the overall sound pressure level at influencing transition.

CONCLUSIONS AND RECOMMENDATIONS

Stability analysis of existing experimental data available from the NASA Langley 8-Foot LFC experiment was completed. As a result of this analysis a number of conclusions and recommendations can be made:

1. For the off-design cases analyzed, incompressible linear stability theory correlates with a n-factor for TS waves of approximately 10 at transition.

2. Tollmien-Schlichting amplification was the dominant instability influencing transition for all the cases analyzed while crossflow amplification was negligible.

3. The off-design conditions provided a unique growth pattern in which disturbance amplification was limited to a narrow region near the nose and a stable region dominated the remaining 95 percent chord.

4. The Tollmien-Schlichting n-factors at transition increased slightly as the Mach number increased, which may be due to the changing disturbance spectra within the narrow band of amplified frequencies.

5. The good correlation between n-factors and transition over the broad range of non-ideal test conditions indicates that this method is a reliable design tool for advanced LFC airfoils in subsonic flight.

6. Future LFC wing designs should consider incorporating suction as far forward as possible with the capacity to significantly increase the suction for off-design conditions such as those studied here.

7. Results of this off-design analysis indicate that transition due to surface roughness, and not disturbance amplification, is a problem that increases as the Mach and Reynolds number increase. This oversuction effect could be significant at the design case. Further studies of this phenomenon at the design case is recommended.

8. Future consideration is recommended for examination of compressibility effects on disturbance amplification.

REFERENCES

1. Smith, A. M. O.: Transition, Pressure Gradient and Stability Theory. IX International Congress for Applied Mechanics, Brussels, 1956.

2. Van Ingen, J. L.: A Suggested Semi-Empirical Method for the Calculation of the Boundary Layer Transition Region. Univ. of Technology, Dept. of Aero. Eng. Report UTH-74, Delft, 1956.

3. Viken, J. K.: Aerodynamic Design Considerations and Theoretical Results for a High Reynolds Number Natural Laminar Flow Airfoil. Masters Thesis, George Washington University, January 1983.

4. Runyan, L. J.; and George-Falvy, D.: Amplication Factors at Transition on an Unswept Wing in Free Flight and on a Swept Wing in Wind Tunnel. AIAA Paper 79-0267, January 1979.

5. Harvey, W. D.; and Pride, J. D.: The NASA Langley Laminar Flow Control Experiment. AIAA Paper 82-0567, March 1982.

6. Fox, R. W.; and McDonald, A. T.: Introduction to Fluid Mechanics. New York: John Wiley and Sons, Inc., 1978.

7. Mack, L. M.: On the Application of Linear Stability Theory to the Problem of Supersonic Boundary-Layer Transition. AIAA Paper 74-134, 1974.

8. Drazin, P. G.; and Reid, W. H.: Hydrodynamic Stability. New York: Cambridge University Press, 1981.

9. Rosenhead, L., ed.: Laminar Boundary Layers. Oxford: Oxford University Press, 1963.

10. Jaffe, N. A.; Okamura, T. T.; and Smith, A. M. O.: Determination of Spatial Amplification Factors and Their Application to Transition. AIAA Journal, vol. 8, 1970, pp. 301-308.

11. Hefner, J. N.; and Bushnell, D. M.: Application of Stability Theory to Laminar Flow Control. AIAA Paper 79-1493, July 1979.

12. Betchov, R.; and Crminale, W. O., Jr.: Stability of Parallel Flows. Academic Press, Inc., 1967.

13. Dagenhart, J. R.: Amplified Crossflow Disturbances in the Laminar Boundary Layer on Swept Wings with Suction. NASA TP-1902, November 1981.

14. Schlichting, H. (J. Kestin, transl.): Boundary-Layer Theory. New York: McGraw-Hill Book Co., Seventh Edition, 1979.

15. Gregory, N.; Stuart, J. T.; and Walker, W. S.: On the Stability of Three-Dimensional Boundary Layers with Application to the Flow Due to a Rotating Disk. Philos. Trans. Roy. Soc. London, ser. A, vol. 248, no. 943, July 14, 1955, pp. 155-199.

16. Pfenninger, W.: Laminar Flow Control Laminarization. Special Course on Concepts for Drag Reduction, AGARD-R-654, June 1977, pp. 3-1 to 3-75.

17. Srokowski, A. J.; and Orzag, S. A.: Mass Flow Requirements for LFC Wing Design. AIAA Paper 77-1222, August 1977.

18. Brown, W. B.: Numerical Calculation of the Stability of Cross-Flow Profiles in Laminar Boundary Layers on a Rotating Disc and on a Swept-Back Wing and an Exact Calculation of the Stability of the Blasius Velocity Profile. Rep. No. NAI-59-5 (BLC-117) (Contract No. AF33(616)-3168), Northrop Aircraft, Inc., January 1959. (Available from DTIC as AD 314 541.)

19. Mack, L. M.: On the Stability of the Boundary Layer on a Transonic Swept Wing. AIAA Paper 79-0264, January 1979.

20. Kaups, K.; and Cebeci, T.: Compressible Laminar Boundary Layers with Suctions on Swept and Tapered Wings. J. Aircraft, vol. 14, no. 7, July 1977, pp. 661-667.

21. Pfenninger, W.; Reed, H. L.; and Dagenhart, J. R.: Design Consideration of Advanced Supercritical Low Drag Suction Airfoils. Viscous Flow Drag Reduction, Gary R. Hough, ed., AIAA, c.1980, pp. 249-271.

22. Allison, D. O.; and Dagenhart, J. R.: Design of a Laminar-Flow-Control Supercritical Airfoil for a Swept Wing. CTOL Transport Technology - 1978, NASA CP-2036, Pt. I, 1978, pp. 395-408.

23. Newman, P. A.; Anderson, E. C.; and Peterson, J. B., Jr.: Numerical Design of the Contoured Wind-Tunnel Linear for the NASA Swept-Wing LFC Test. AIAA Paper 82-0568, March 1982.

24. Spangler, J. G.; and Wells, C. S., Jr.: Effect of Freestream Disturbances on Boundary-Layer Transition. AIAA Journal, vol. 6, 1968, pp. 543-545.

25. Mack, L. M.: Transition and Laminar Instability. JPL Publication 77-15, 1977.

26. Stainback, P. C.; and Owen, F. K.: Dynamic Flow Quality Measurements in the Langley Low Turbulence Pressure Tunnel. AIAA Paper 84-0621, March 1984.

27. Bobbitt, P. J.; Waggoner, E. G.; Harvey, W. D.; and Dagenhart, J. R.: A Faster "Transition" to Laminar Flow. SAE Paper No. 851855, presented at Aerospace Technology Conference & Exposition, Long Beach, California, October 14, 1985.

28. Pfenninger, W.: Experiments with Laminar Flow in the Inlet Length of a Tube at High Reynolds Numbers with and without Boundary Layer Suction. Norair Division Report, May 1952, Northrop Corp., Hawthorne, CA.

29. Pfenninger, W.; and Bacon, J. W., Jr.: Influence of Acoustical Disturbances on the Behavior of a Swept Laminar Suction Wing. Rept. NOR 62-124 (BLC-141), October 1962, Northrop Corp., Hawthorne, CA.

30. Carlson, J. C.; and Bacon, J. W., Jr.: Influence of Acoustical Disturbances in the Suction Ducting System on the Laminar Flow Control Characteristics of a 33° Swept Suction Wing. Rept. NOR 65-232, August 1965.

31. Carlson, J. C.: Investigation of the Laminar Flow Control Characteristics of a 33° Swept Suction Wing at High Reynolds Numbers in the NASA Ames 12-Foot Pressure Tunnel in August 1965. Rept. NOR 66-58, January 1966.

APPENDIX

Development of RSL Parameter

The laminar boundary-layer thickness is known to vary with Reynolds number as (ref. 14)

$$\delta/c \sim 1/\sqrt{R_c} \, . \tag{1}$$

In order to remove the same fraction of the boundary layer for various test Reynolds numbers, the suction coefficient should also vary as the boundary-layer thickness varies

$$C_Q \sim \delta/c \sim 1/\sqrt{R_c} \, . \tag{2}$$

Therefore, for the same fraction of the boundary layer removed for a test case compared to a design case we have

$$C_{Q_{REF}} \sqrt{R_{c_{REF}}} = C_{Q_{DES}} \sqrt{R_{c_{DES}}} \, . \tag{3}$$

The design integrated suction coefficient is defined as

$$\tilde{C}_{Q_{DES}} = \int_0^1 C_{Q_{DES}} (x/c) d(x/c). \tag{4}$$

The object is to remove the Reynolds number dependence from the suction parameter. Therefore the integrated suction coefficient for the case of interest shall be compared to a reference integrated suction value that is scaled by the Reynolds number. Thus the Reference Suction Level (RSL) parameter is defined as

$$RSL = \hat{C}_Q \; / \; \hat{C}_{Q_{REF}} \tag{5}$$

where the integrated suction coefficient of interest is

$$\hat{C}_Q = \int_0^1 C_Q(x/c)d(x/c) \tag{6}$$

and the reference integrated suction level is the design suction level scaled by the Reynolds number difference

$$\hat{C}_{Q_{REF}}(R_c) = \hat{C}_{Q_{DES}} \sqrt{R_{c_{DES}} / R_c} \; . \tag{7}$$

The design suction distribution and overall level is shown in figure 8. Based on the integrated suction value for the design case, equation (7) was used to generate the reference levels as shown in the table

R_c	$\hat{C}_{Q_{REF}}$
10 million	-0.00049
12	-0.00045
14	-0.00042
16	-0.00039
18	-0.00037
20	-0.00035

These reference values were used in conjunction with equation (5) to find the RSL for each case.

TEST CASE	M_∞	R_e	RSL	LAM/TURB	MAX AMP FREQUENCY	INCOMP n_{TS}(fwd)	MAX AMP WAVE LENGTH	INCOMP n_{CF}(fwd)	MAX AMP WAVE LENGTH	INCOMP n_{CF}(MID)
917-13-3	.4	10	3.112	LAM	11000	3.381	.0005	.437	-	0
917-13-5	.4	10	1.436	LAM	9000	7.234	.0005	.432	-	0
917-36-6	.4	10	1.192	TURB	9000	8.756	.0005	.470	-	0
917-13-8	.4	12	1.9448	LAM	12000	6.63	.0004	.793	-	0
917-13-9	.4	12	1.516	LAM	9000	8.108	-	-	-	-
917-13-10	.4	12	1.296	TURB	9000	9.104	-	-	-	-
917-13-13	.4	14	2.211	LAM	11000	6.359	-	-	-	-
917-13-15	.4	14	1.811	LAM	12000	7.472	-	-	-	-
917-13-17	.4	16	2.34	LAM	12000	6.898	-	-	-	-
917-13-18	.4	16	1.777	LAM	10000	8.547	-	-	-	-
917-14-2	.4	18	2.76	LAM	16000	5.768	.0004	1.768	.0012	.084
917-14-4	.4	18	2.09	LAM	13000	7.928	.0004	1.795	.0014	.109
917-14-5	.4	18	1.77	70/80%	11000	9.673	.0004	1.858	.0016	.123
917-14-6	.4	20	2.71	TURB*	17000	6.214	.0003	2.127	.0012	.079
917-14-7	.4	20	2.56	TURB*	11000	6.599	.0003	2.122	.0012	.072
917-10-4	.6	10	1.844	LAM	14000	7.413	-	-	-	-
917-10-5	.6	10	1.505	LAM	14000	8.435	-	-	-	-
917-10-7	.6	10	1.374	LAM	14000	9.014	-	-	-	-
917-10-8	.6	10	1.313	LAM	14000	9.157	-	-	-	-
917-10-9	.6	10	1.255	90%	11000	9.709	-	-	-	-
917-10-10	.6	10	1.250	~85%	11000	9.840	-	-	-	-
917-10-11	.6	10	1.211	~25%	12000	10.105	-	-	-	-
917-10-12	.6	10	1.188	~20%	12000	10.174	-	-	-	-
917-10-13	.6	10	1.518	TURB	12000	10.516	-	-	-	-
917-10-14	.6	10	1.128	TURB	12000	10.531	-	-	-	-
917-10-15	.6	10	1.092	TURB	12000	10.958	-	-	-	-
917-10-16	.6	10	.860	TURB	1000	13.727	-	-	-	-
917-10-17	.6	12	2.038	LAM	14000	7.686	-	-	-	-
917-10-18	.6	12	1.927	LAM	14000	7.905	-	-	-	-
917-10-19	.6	12	1.645	LAM	15000	8.979	-	-	-	-

Table 1.- Tabulated results of incompressible stability analysis.

TEST CASE	M_∞	R_e	RSL	LAM/TURB	MAX AMP FREQUENCY	INCOMP n_{TS}(fwd)	MAX AMP WAVE LENGTH	INCOMP n_{CF}(fwd)	MAX AMP WAVE LENGTH	INCOMP n_{CF}(MID)
917-10-20	.6	12	1.495	LAM	14000	9.512	-	-	-	-
917-10-21	.6	12	1.422	~90%	14000	9.848	-	-	-	-
917-10-22	.6	12	1.353	TURB	11000	10.303	-	-	-	-
917-10-23	.6	12	1.305	TURB	12000	10.954	-	-	-	-
917-10-24	.6	12	1.274	TURB	12000	11.104	-	-	-	-
917-10-25	.6	12	1.101	TURB	10000	12.315	-	-	-	-
917-10-26	.6	12	.943	TURB	11000	15.142	.0005	1.074	.0020	1.412
917-10-27	.6	14	2.213	LAM	14000	7.759	.0004	1.461	.0017	.017
917-10-28	.6	14	1.829	LAM	15000	9.254	-	-	-	-
917-10-29	.6	14	1.653	LAM	15000	9.926	-	-	-	-
917-10-30	.6	14	1.595	LAM	15000	10.427	-	-	-	-
917-10-31	.6	14	1.500	~25%	15000	10.698	-	-	-	-
917-10-32	.6	14	1.473	TURB	15000	10.845	-	-	-	-
917-10-33	.6	14	1.364	TURB	15000	11.493	.0004	1.483	.0017	1.033
917-10-34	.6	16	2.046	~90%*	19000	7.835	.0004	1.832	-	-
917-10-35	.6	16	2.090	LAM	15000	8.856	-	-	-	-
917-10-36	.6	16	1.917	LAM	16000	9.618	-	-	-	-
917-10-37	.6	16	1.687	~90%	16000	10.597	-	-	-	-
917-10-38	.6	16	1.450	TURB	16000	12.100	.0004	1.852	.0017	1.210
917-10-39	.6	18	2.565	~85%*	19000	7.833	.0004	2.211	-	-
917-10-40	.6	18	2.158	~90%*	16000	8.993	.0004	2.246	.0014	.209
917-10-41	.6	18	2.006	LAM	16000	9.636	.0004	2.263	.0014	.433
917-10-42	.6	18	1.803	~90%	16000	10.630	.0004	2.268	.0014	.680
917-10-43	.6	18	1.721	~20%	16000	11.194	.0004	2.248	.0014	.941
917-10-44	.6	18	1.607	TURB	13000	12.079	.0004	2.256	.0014	1.217
917-10-45	.6	20	2.734	~85%*	18000	7.668	.0004	2.538	-	-
917-10-46	.6	20	2.224	~85%*	15000	9.259	.0004	2.569	.0014	.298
917-10-47	.6	20	2.011	LAM	17000	10.327	.0004	2.577	.0014	.618
917-10-48	.6	20	1.809	TURB	16000	11.437	.0004	2.597	.0014	1.041
917-13-49	.6	20	1.7765	TURB	17000	11.723	.0004	2.586	.0014	1.147

Table 1.- Continued.

TEST CASE	M_∞	R_e	RSL	LAM/TURB	MAX AMP FREQUENCY	INCOMP n_{TS}(fwd)	MAX AMP WAVE LENGTH	INCOMP n_{CF}(fwd)	MAX AMP WAVE LENGTH	INCOMP n_{CF}(MID)
917-11-10	.7	10	1.445	LAM	13000	8.992	.0006	.938	.0022	.639
917-11-11	.7	10	1.265	LAM	14000	9.721	-	-	-	-
917-11-12	.7	10	1.121	TURB	11000	10.719	.0006	.924	.0024	.979
917-11-13	.7	10	.929	TURB	8000	13.604	.0006	.945	.0026	1.418
917-11-14	.7	10	.930	TURB	10000	13.226	.0006	.916	.0024	1.327
917-11-15	.7	10	.786	TURB	8000	16.450	.0006	.941	.0026	1.775
917-12-2	.7	12	1.628	LAM	14000	9.180	.0005	1.381	.0020	.755
917-12-3	.7	12	1.545	LAM	14000	9.271	.0005	1.344	.0020	.868
917-12-4	.7	12	1.451	LAM	14000	9.665	.0005	1.393	.0022	.866
917-12-5	.7	12	1.287	TURB	15000	10.829	.0005	1.423	.0200	1.236
917-12-6	.7	12	1.132	TURB	10000	12.195	.0005	1.388	.0022	1.530
917-12-7	.7	12	1.024	TURB	10000	14.013	.0005	1.392	.0022	1.794
917-12-9	.7	14	1.766	LAM	18000	9.217	.0005	1.778	.0018	.849
917-12-10	.7	14	1.676	LAM	14000	9.724	.0005	2.054	.0017	.970
917-12-11	.7	14	1.59	LAM	14000	9.966	.0005	2.018	.0017	1.073
917-12-12	.7	14	1.478	~70%	15000	10.792	.0005	2.004	.0017	1.302
917-12-17	.7	16	1.943	~85%*	19000	9.480	.0004	2.479	.0017	.881
917-12-18	.7	16	1.809	~90%*	19000	9.682	.0004	2.559	.0017	1.019
917-12-19	.7	16	1.682	~90%	15000	10.601	.0004	2.557	.0017	1.230
917-12-20	.7	16	1.603	TURB	15000	11.215	.0004	2.514	.0017	1.398
917-12-21	.7	16	1.505	TURB	15000	11.980	.0004	2.565	.0017	1.768
917-12-22	.7	18	2.067	~85%*	20000	9.403	.0004	2.971	.0014	.968
917-12-23	.7	18	1.944	~90%*	20000	9.705	.0004	3.045	.0014	1.150
917-12-24	.7	18	1.903	~90%*	20000	9.765	.0004	3.014	.0014	1.174
917-12-25	.7	18	1.734	60-70%	15000	11.089	.0004	2.983	.0014	1.452
917-12-26	.7	18	1.650	TURB	15000	11.747	.0004	3.006	.0014	1.745
917-12-27	.7	20	2.202	~85%*	20000	9.361	.0004	3.380	.0012	.885
917-12-28	.7	20	2.049	~85*	20000	9.583	.0004	3.466	.0014	1.005
917-12-29	.7	20	1.788	TURB	20000	11.046	.0004	3.483	.0014	1.668
917-12-30	.7	20	1.629	TURB	16000	12.883	.0004	3.475	.0014	2.254

Table 1.- Concluded.

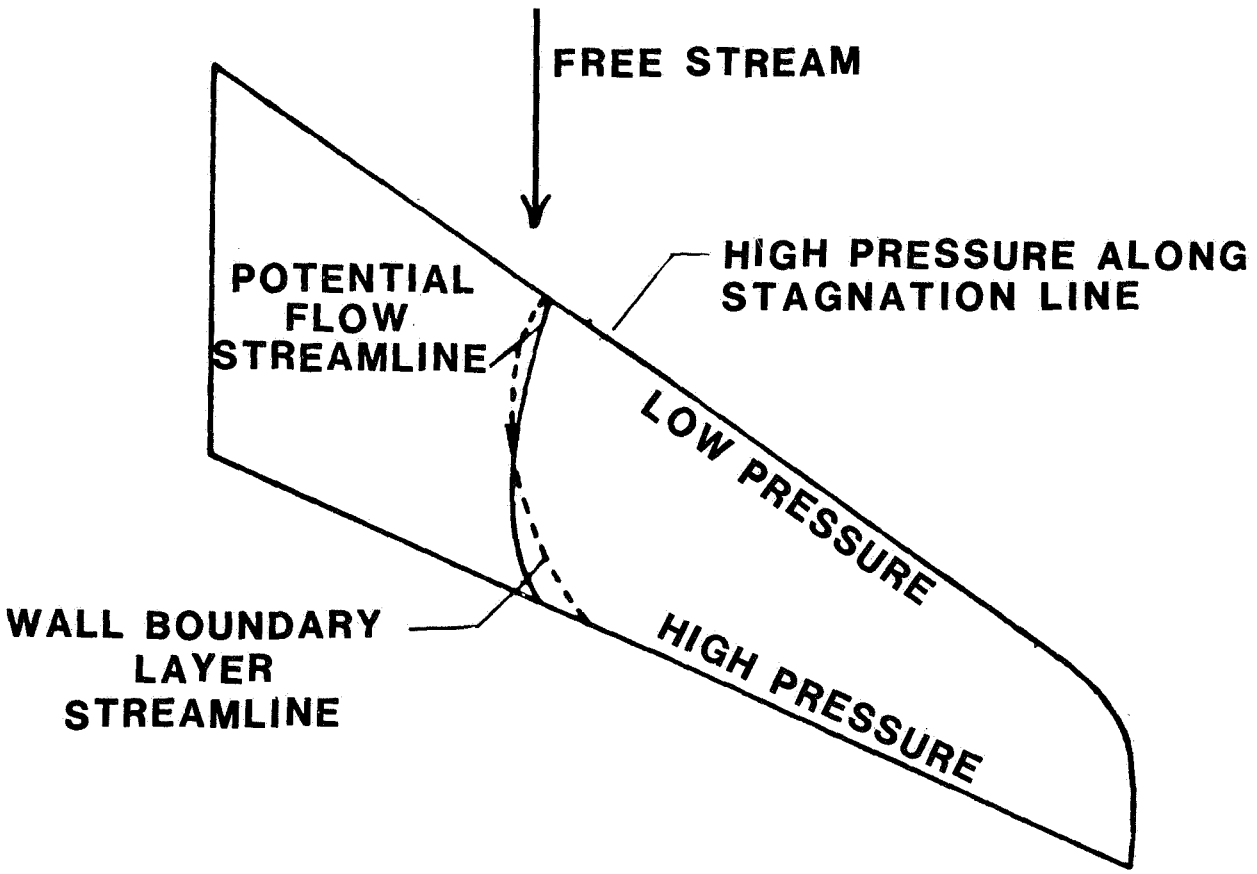

Figure 1.- Flow conditions on typical sweptback wing.

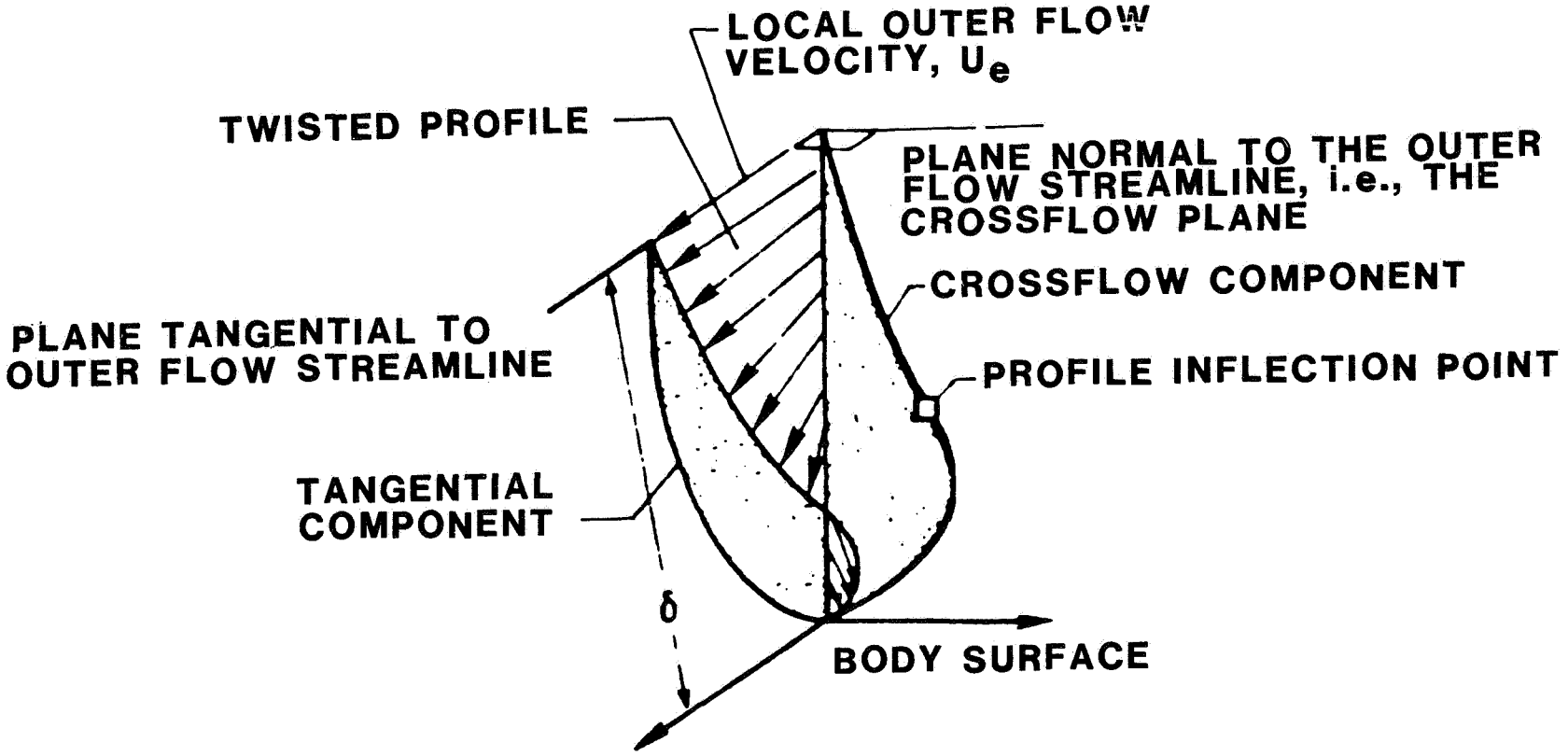

Figure 2.- Swept-wing boundary-layer profile.

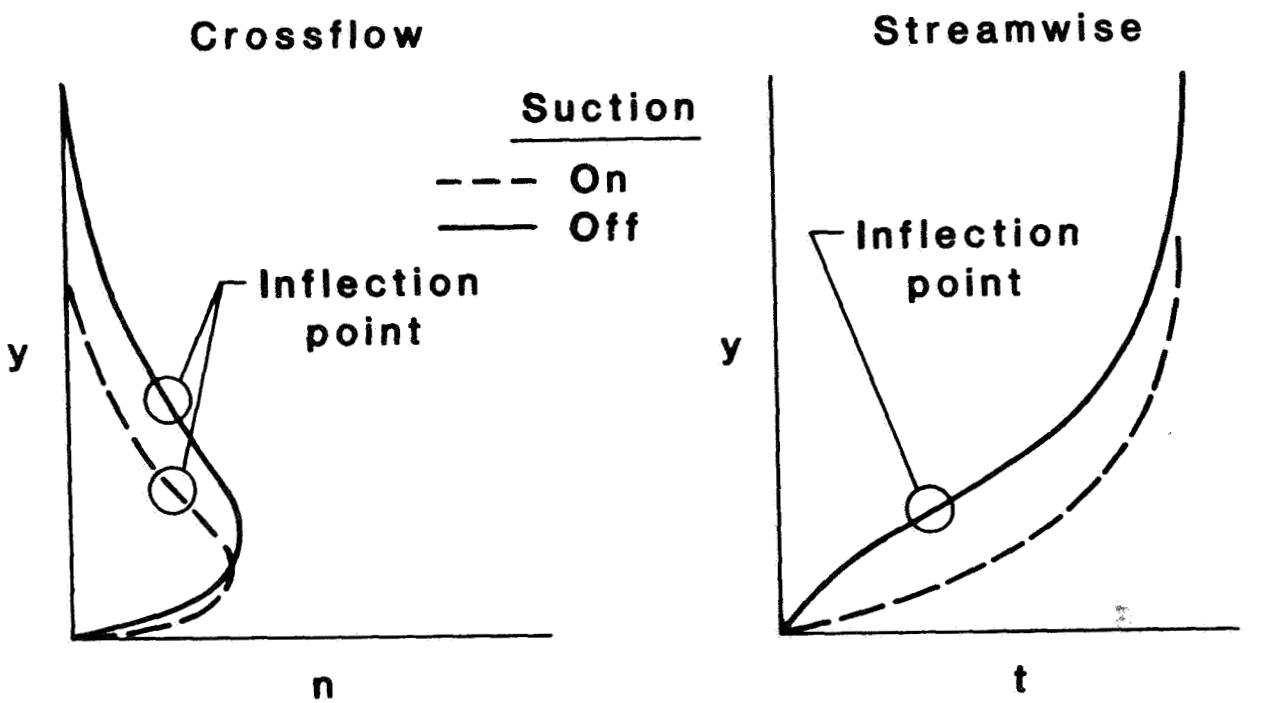

Figure 3.- Effect of suction on streamwise and crossflow boundary layer profiles.

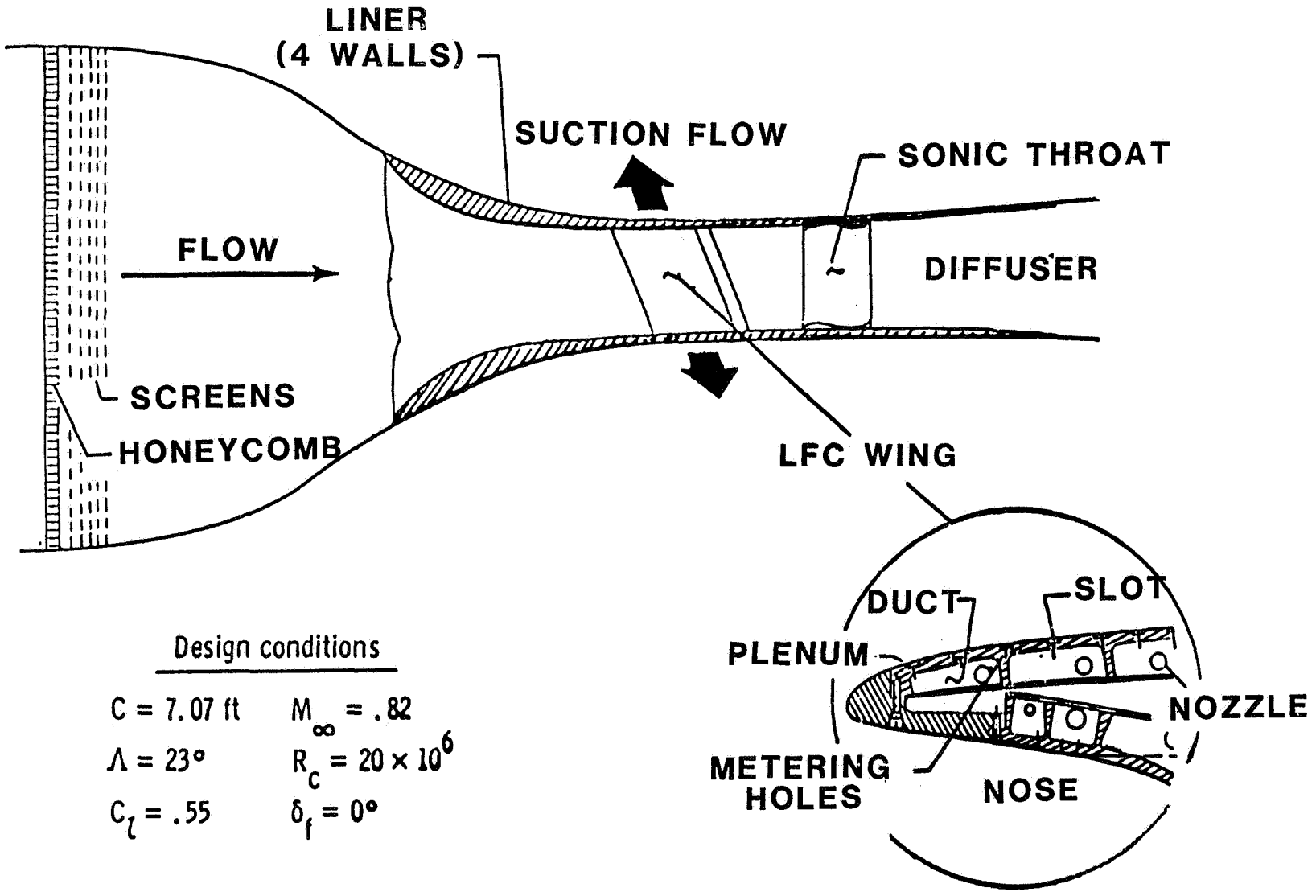

Figure 4.-Schematic of the tunnel and model for LFC experiment in the NASA Langley 8-ft Transonic Pressure Tunnel.

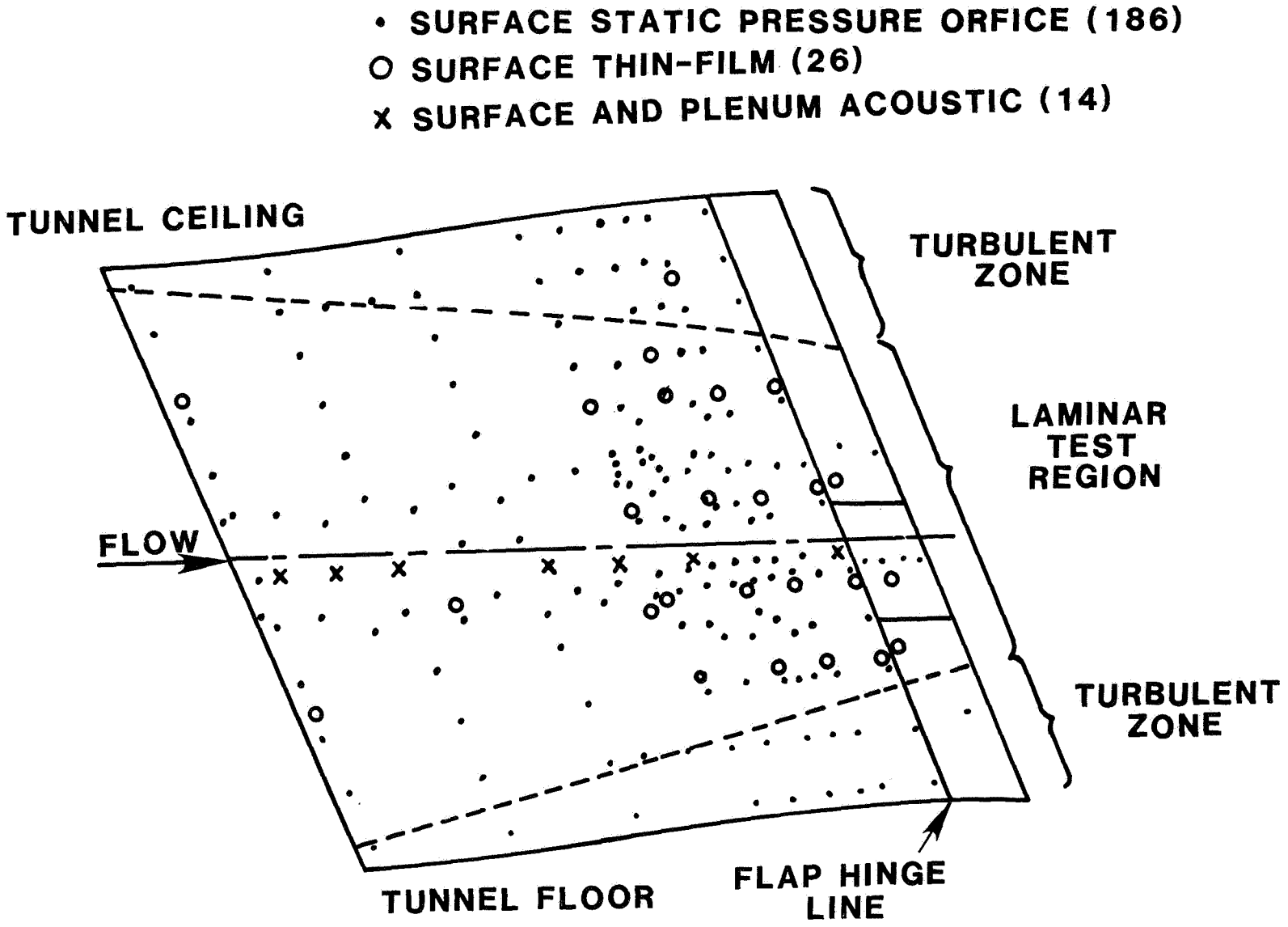

Figure 5.- Schematic of instrumentation locations on upper surface of LFC model.

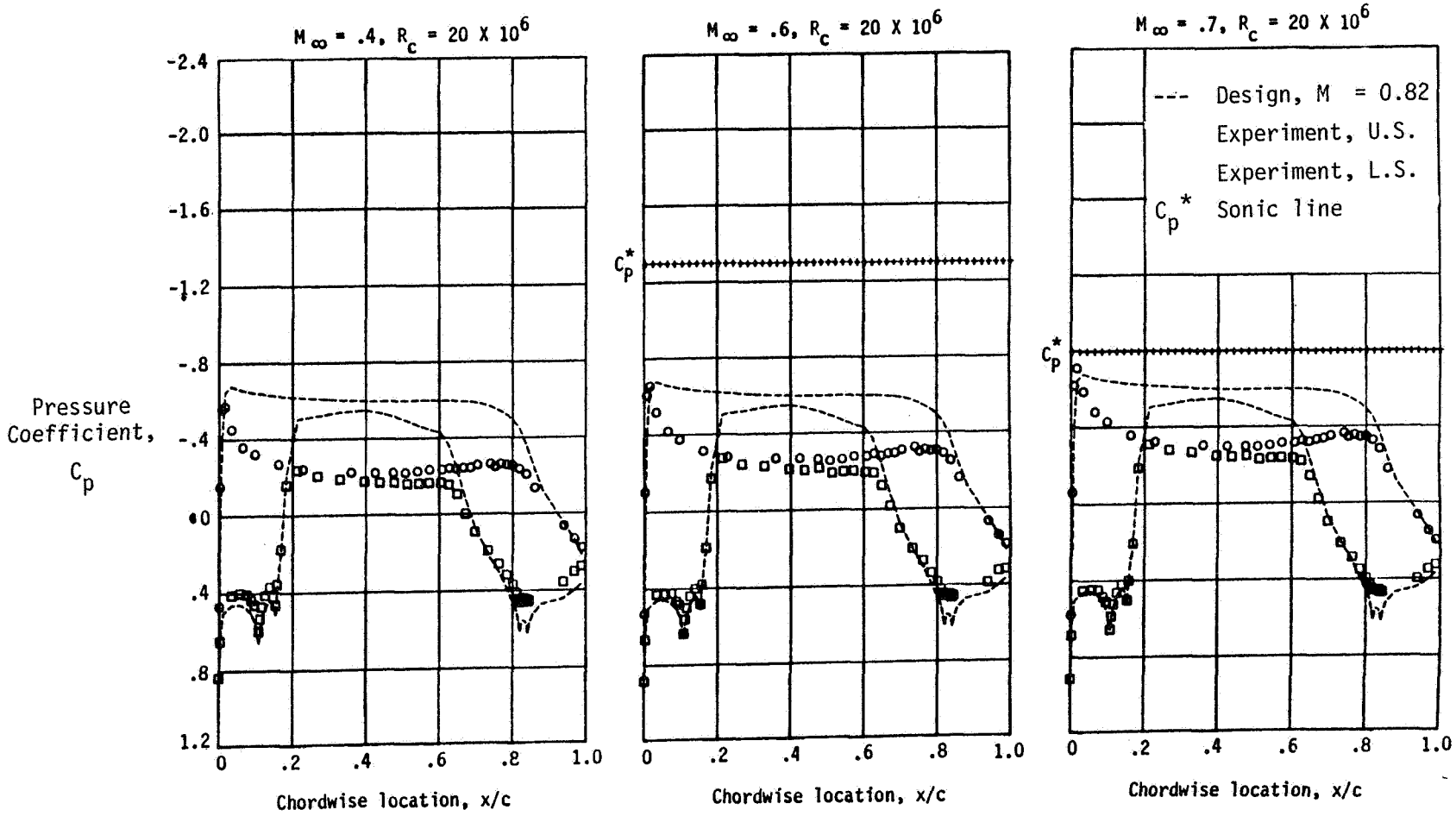

Figure 6.- Sample chordwise pressure distributions along center span of the LFC model.

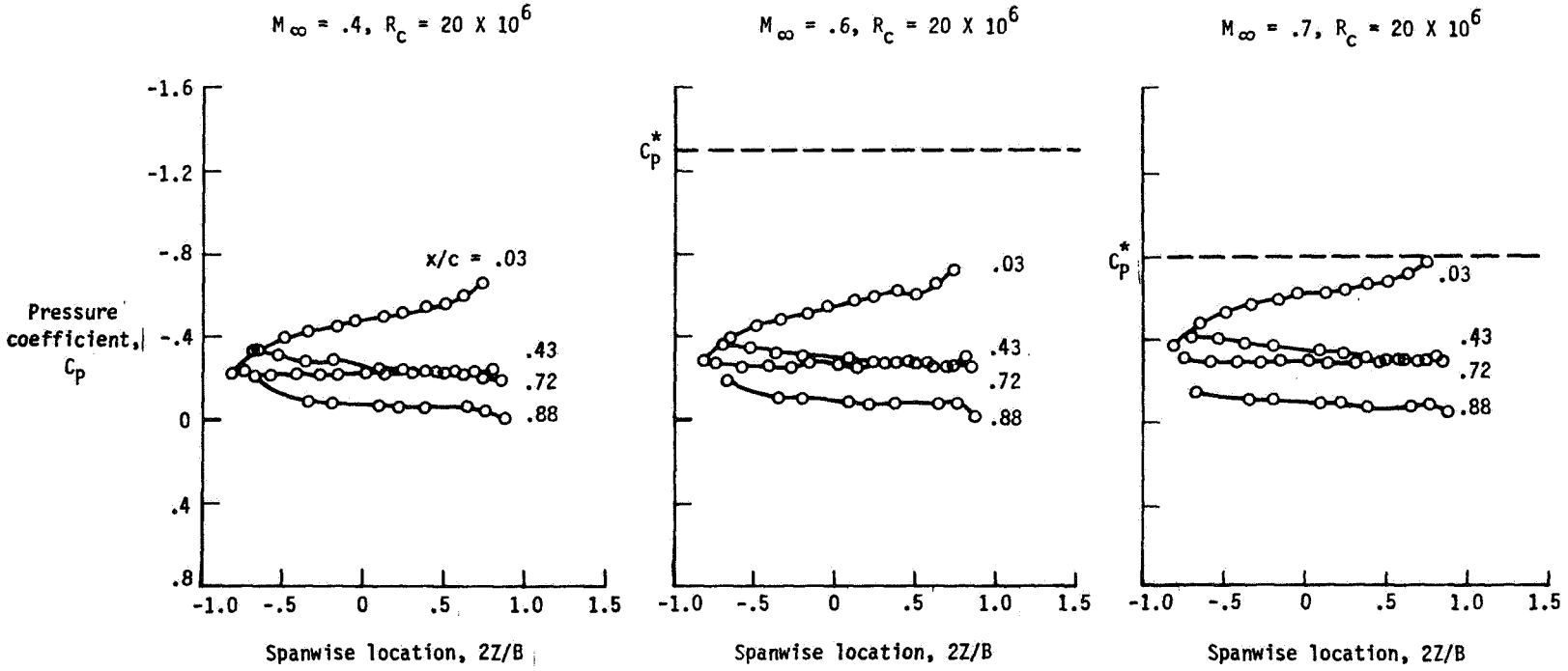

Figure 7.- Sample spanwise pressure distributions for various chord locations.

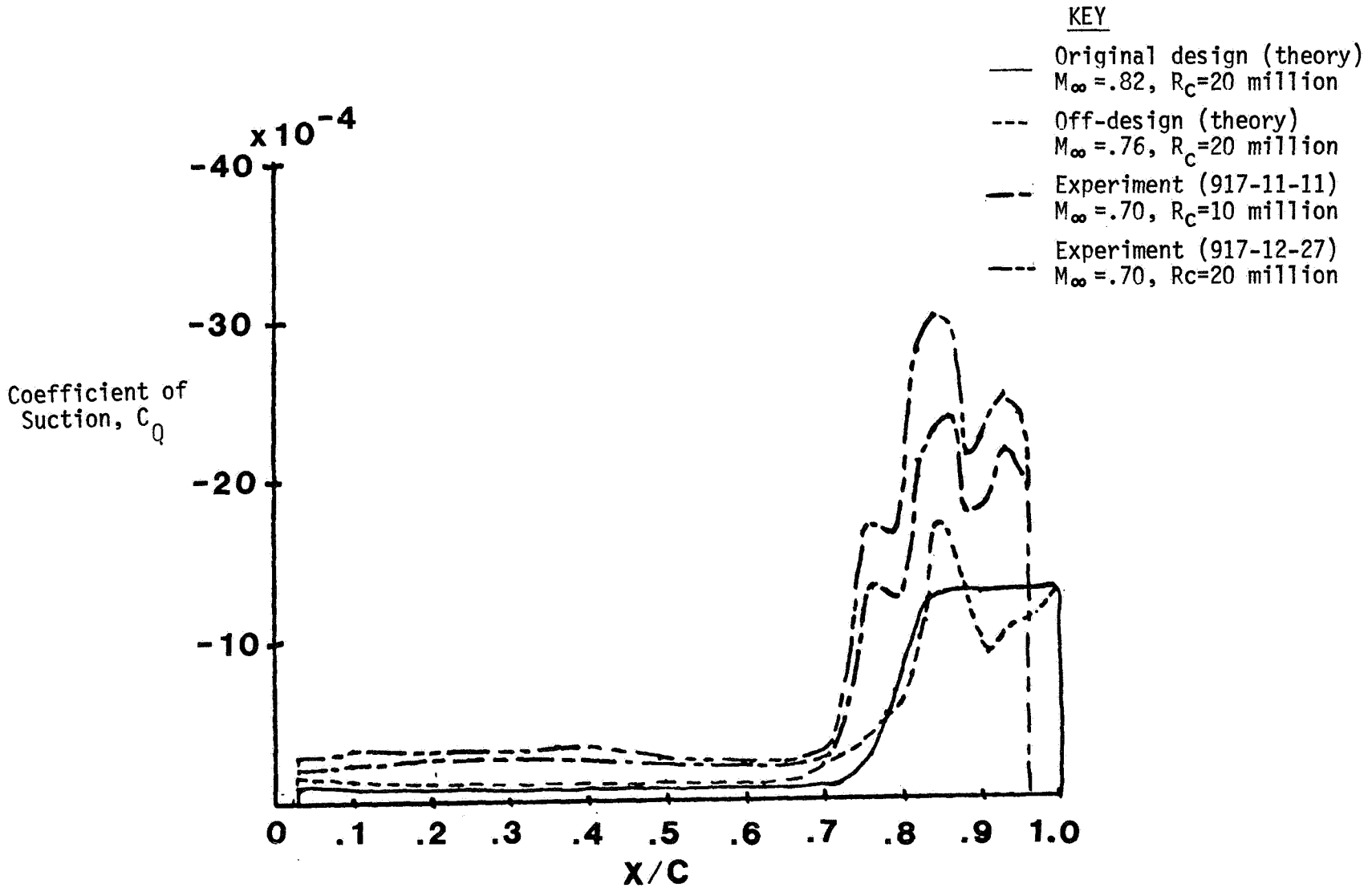

Figure 8.- Comparisons of theoretical and experimental suction distributions.

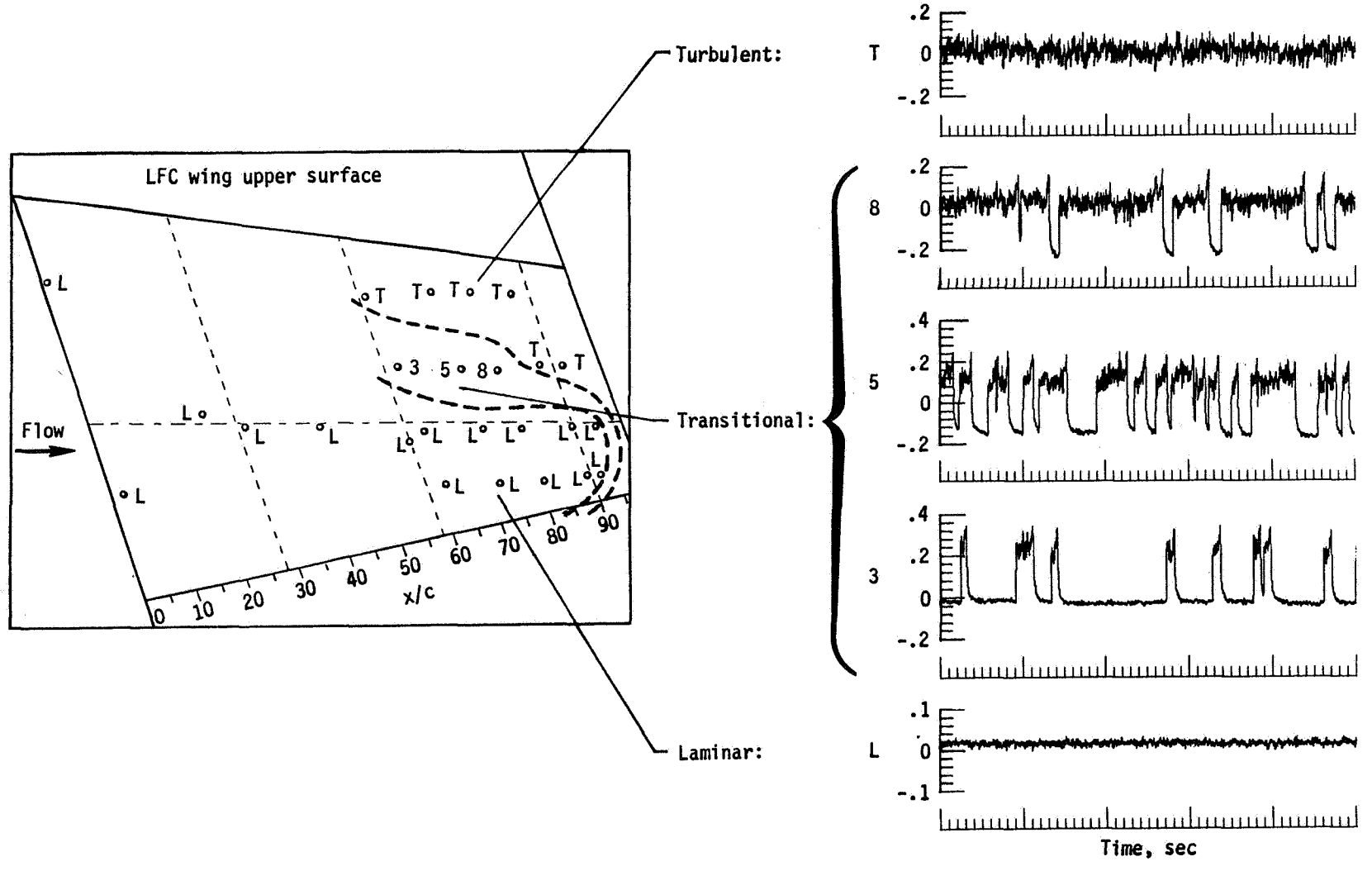

Figure 9.- Example hot-film signals and corresponding locations on upper surface of LFC model.

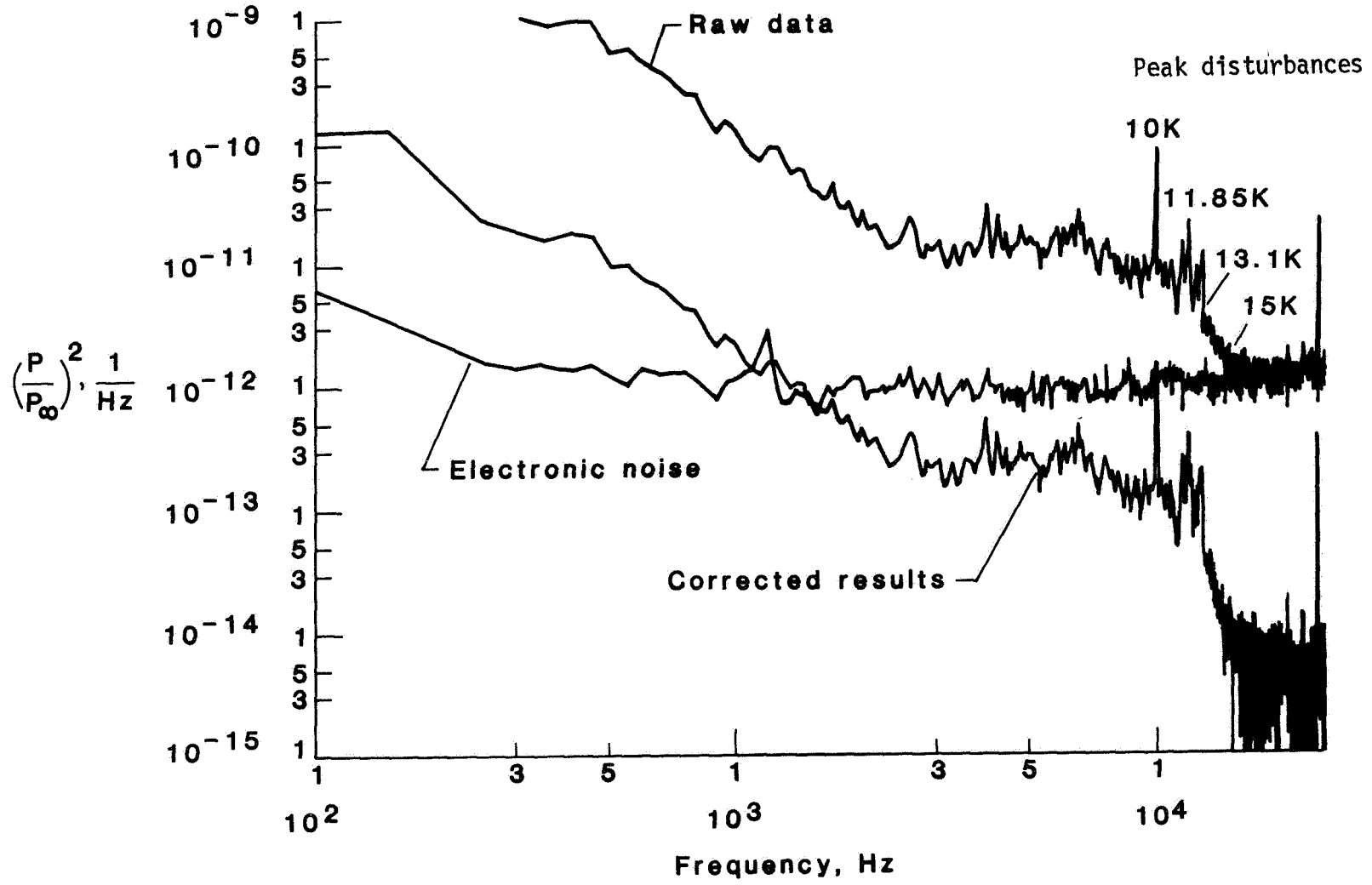

Figure 10.- Sample free-stream acoustic data for LFC test, M_∞=.4 and R_c=10 million.

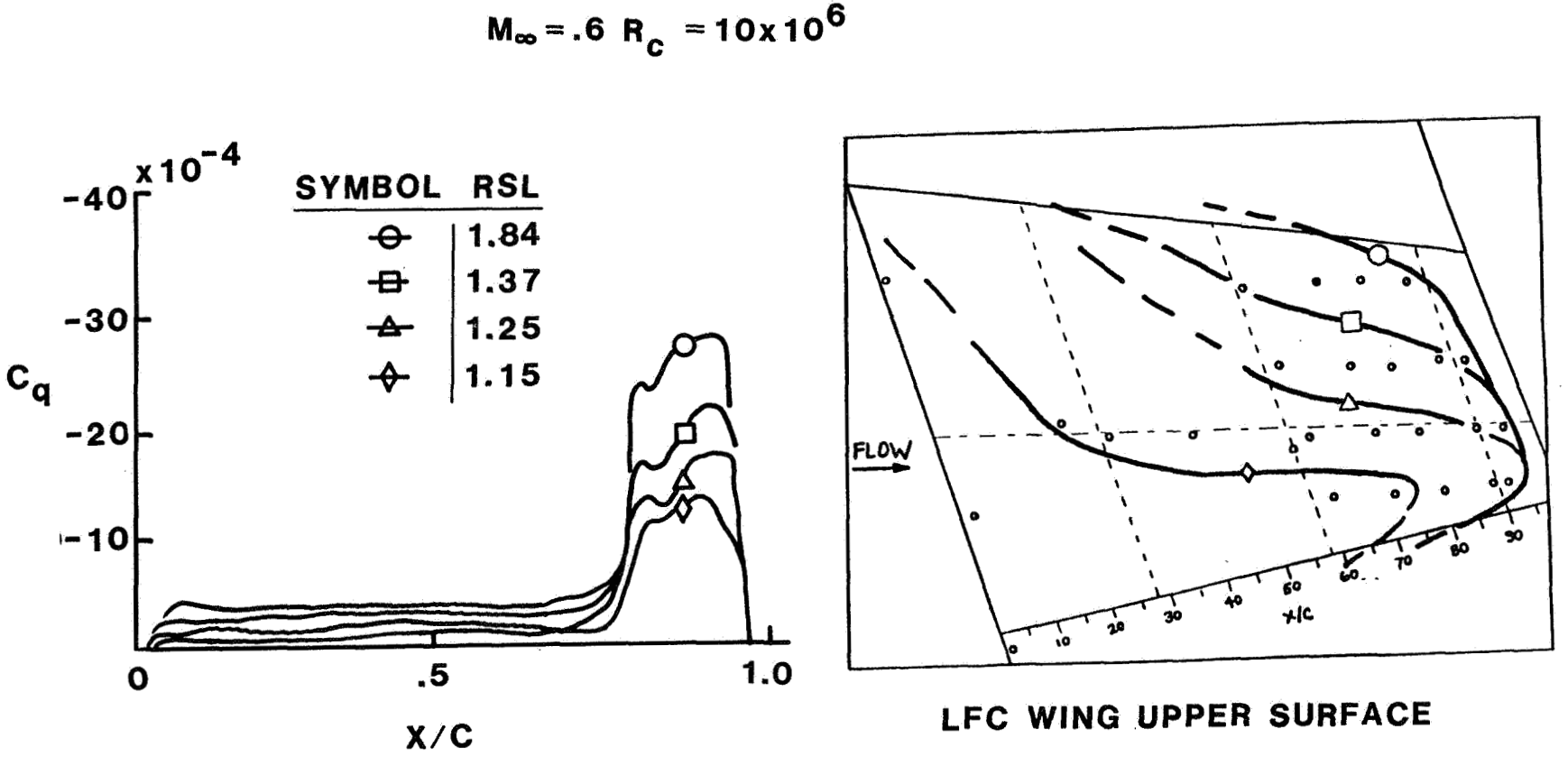

Figure 11.- Effect of suction excursion on transition pattern, $M_\infty = .6$ and $R_c = 10$ million.

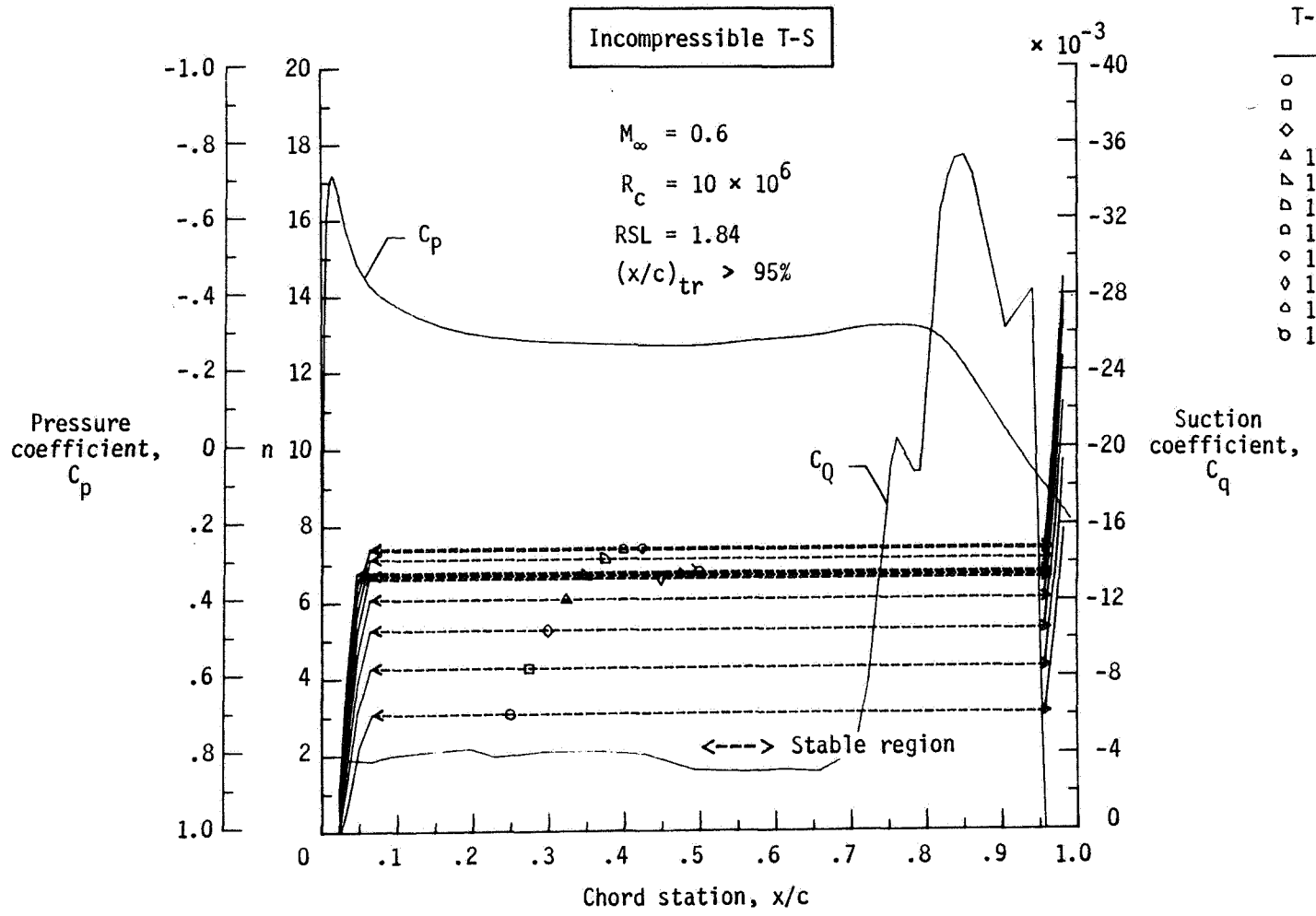

T-S freq., Hz	n_{max}
7000	3.1
8000	4.3
9000	5.3
10 000	6.1
11 000	6.7
12 000	7.1
13 000	7.4
14 000	7.4
15 000	6.6
16 000	6.7
17 000	6.8

Figure 12(a).- Incompressible TS calculations for case 1, M_∞ = 0.6, R_c = 10 million and RSL = 1.84.

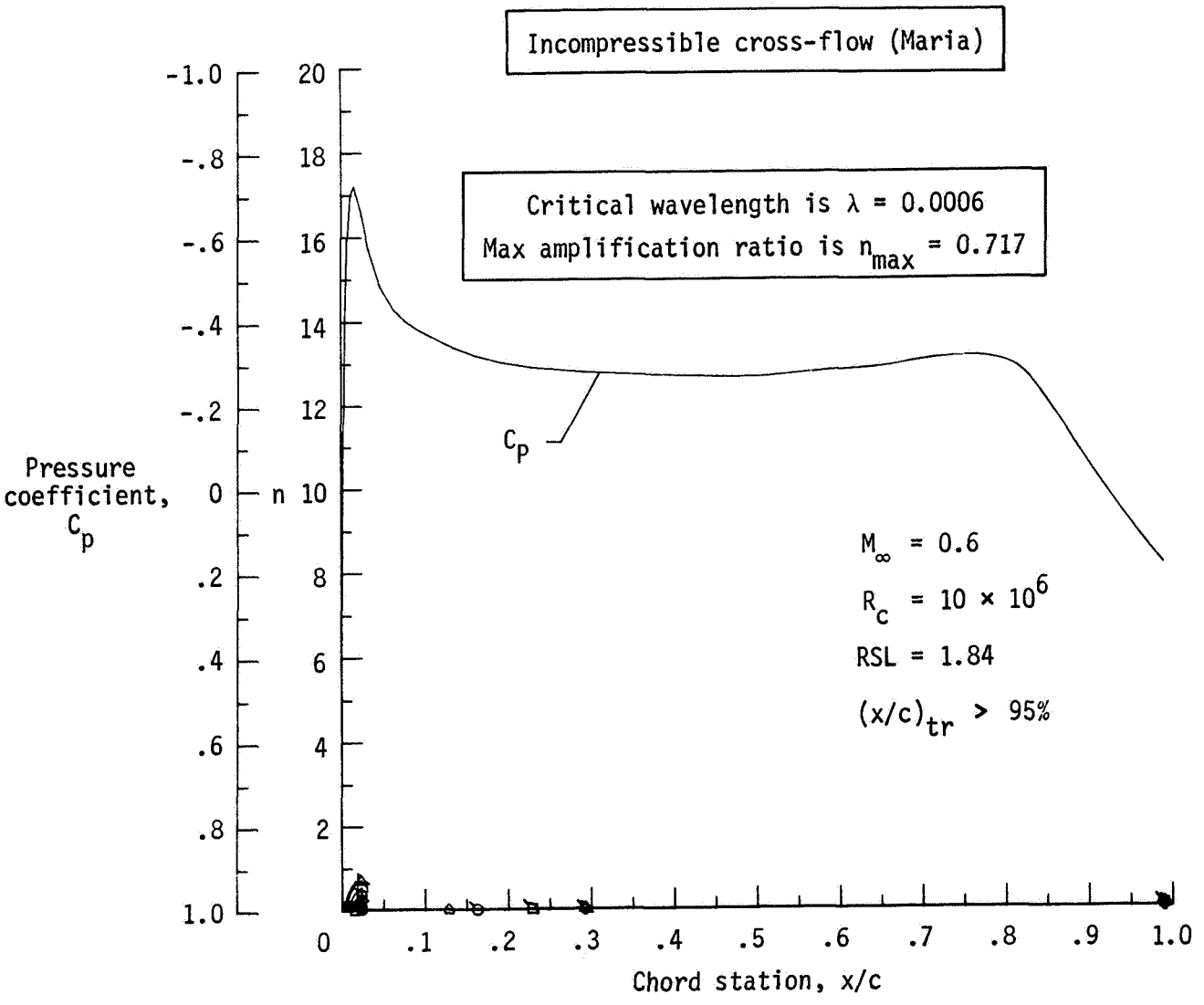

Figure 12(b).- Incompressible CF calculations for case 1, M_∞ = 0.6, R_c = 10 million and RSL = 1.84.

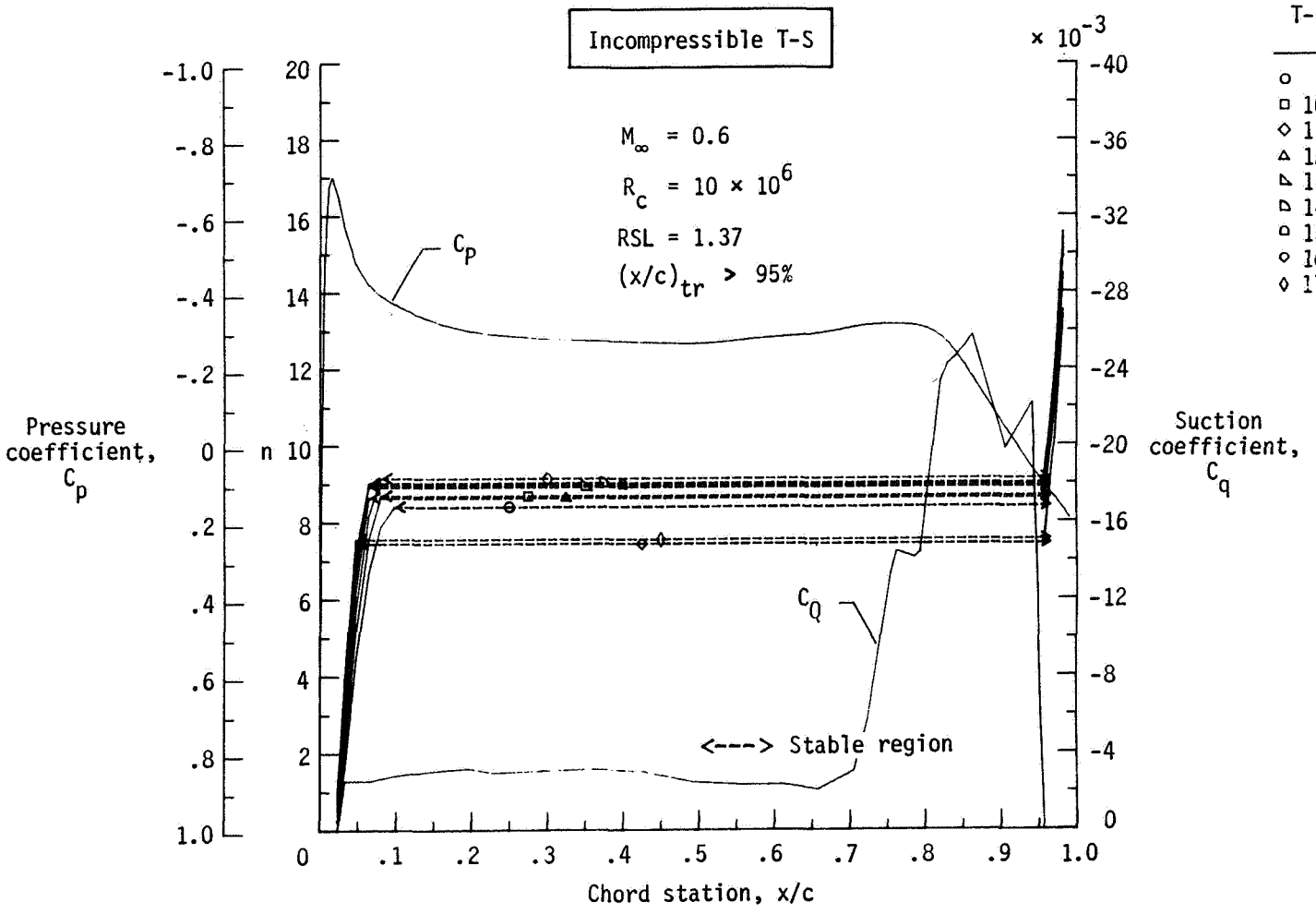

T-S freq., Hz	n_{max}
○ 9000	8.4
□ 10 000	8.7
◇ 11 000	9.1
△ 12 000	8.6
◺ 13 000	8.9
◻ 14 000	9.0
⌓ 15 000	9.0
◇ 16 000	7.4
◇ 17 000	7.5

Figure 13(a).- Incompressible TS calculations for case 2, M_∞ = 0.6, R_c = 10 million and RSL = 1.37.

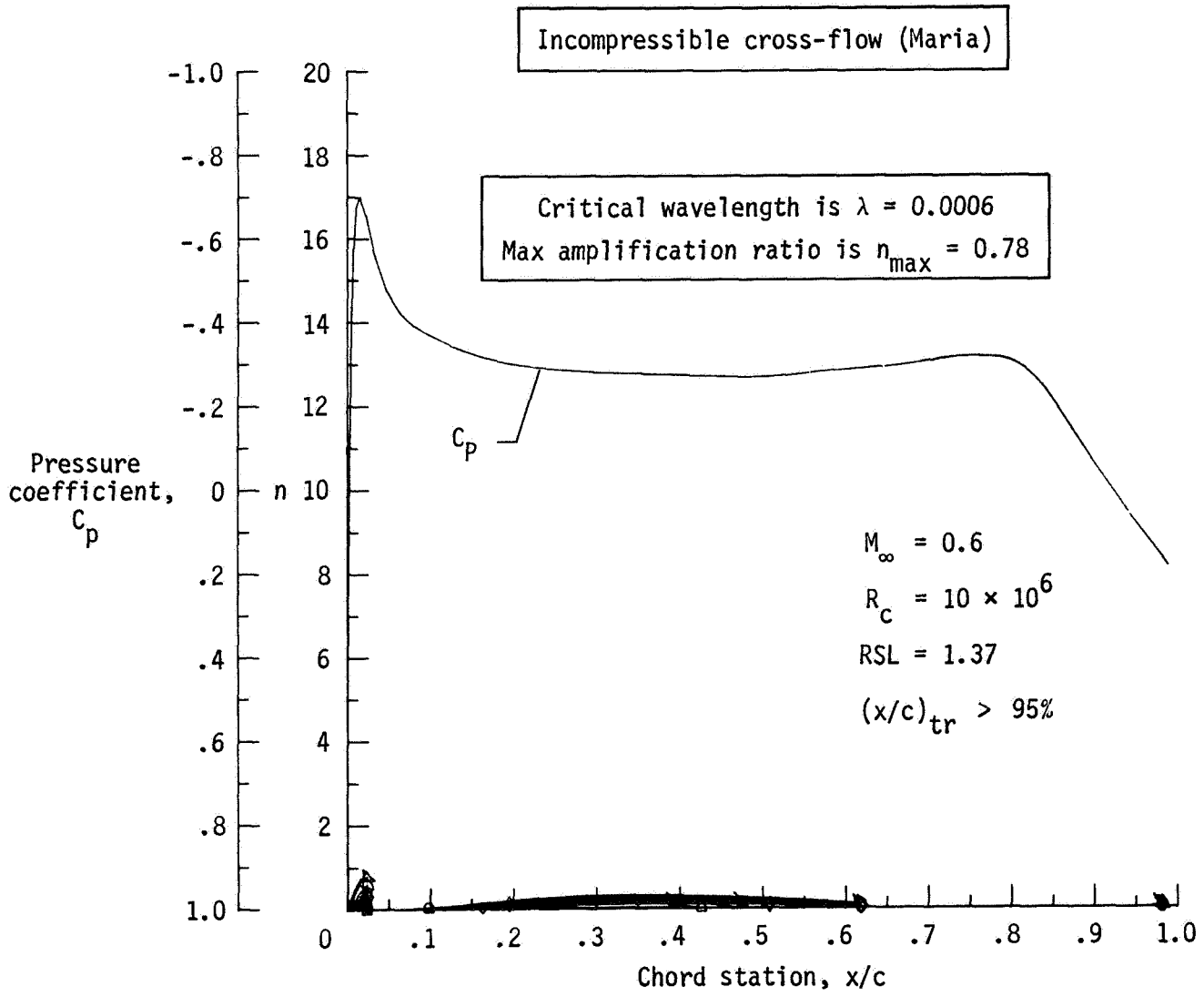

Figure 13(b).- Incompressible CF calculations for case 2, M_∞ = 0.6, R_C = 10 million and RSL = 1.37.

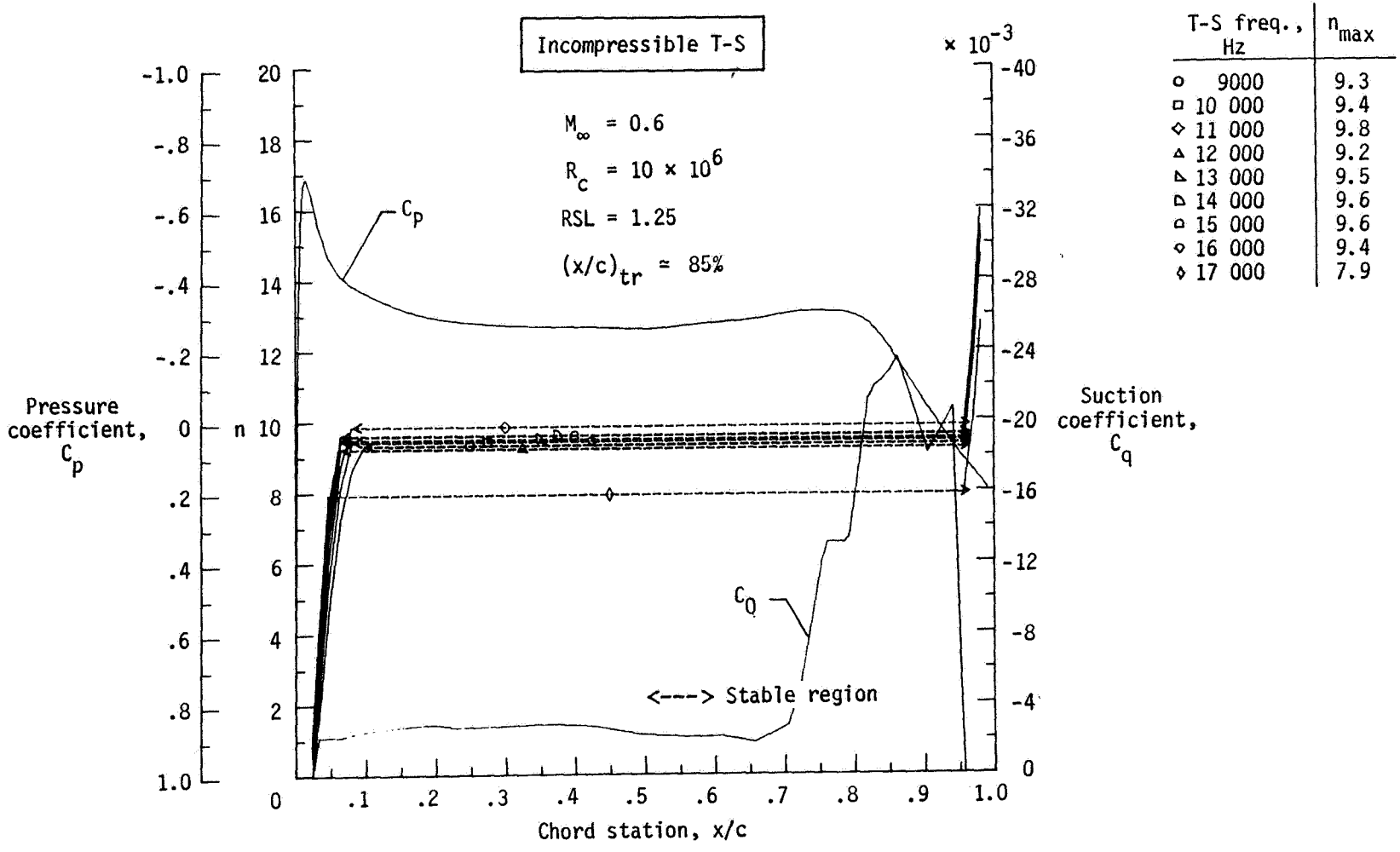

T-S freq., Hz	n_{max}
o 9000	9.3
□ 10 000	9.4
◇ 11 000	9.8
△ 12 000	9.2
▷ 13 000	9.5
▷ 14 000	9.6
▫ 15 000	9.6
◇ 16 000	9.4
◇ 17 000	7.9

Figure 14(a).- Incompressible TS calculations for case 3, M_∞ = 0.6, R_c = 10 million and RSL = 1.25.

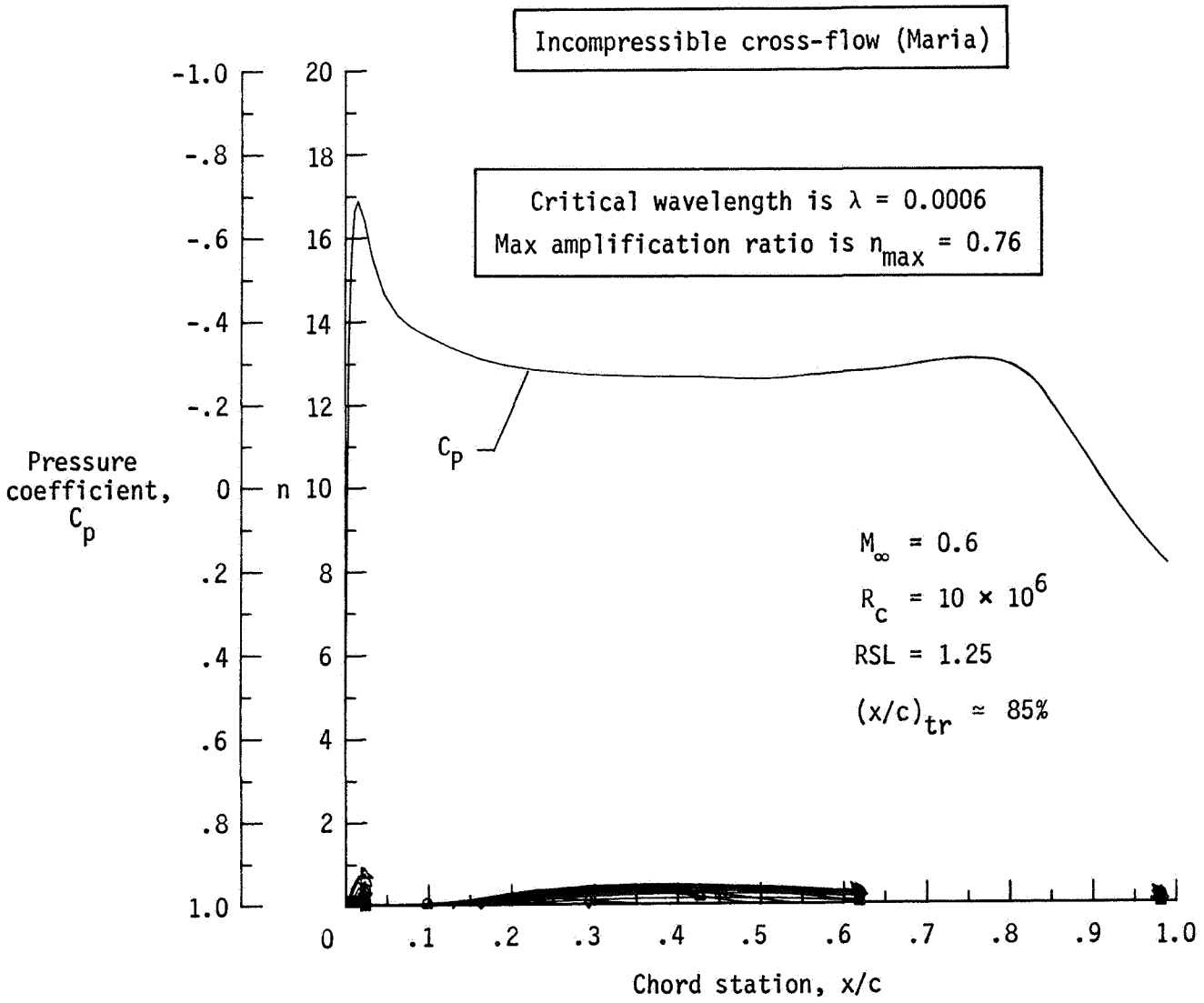

Figure 14(b).- Incompressible CF calculations for case 3, M_∞ = 0.6, R_c = 10 million and RSL = 1.25.

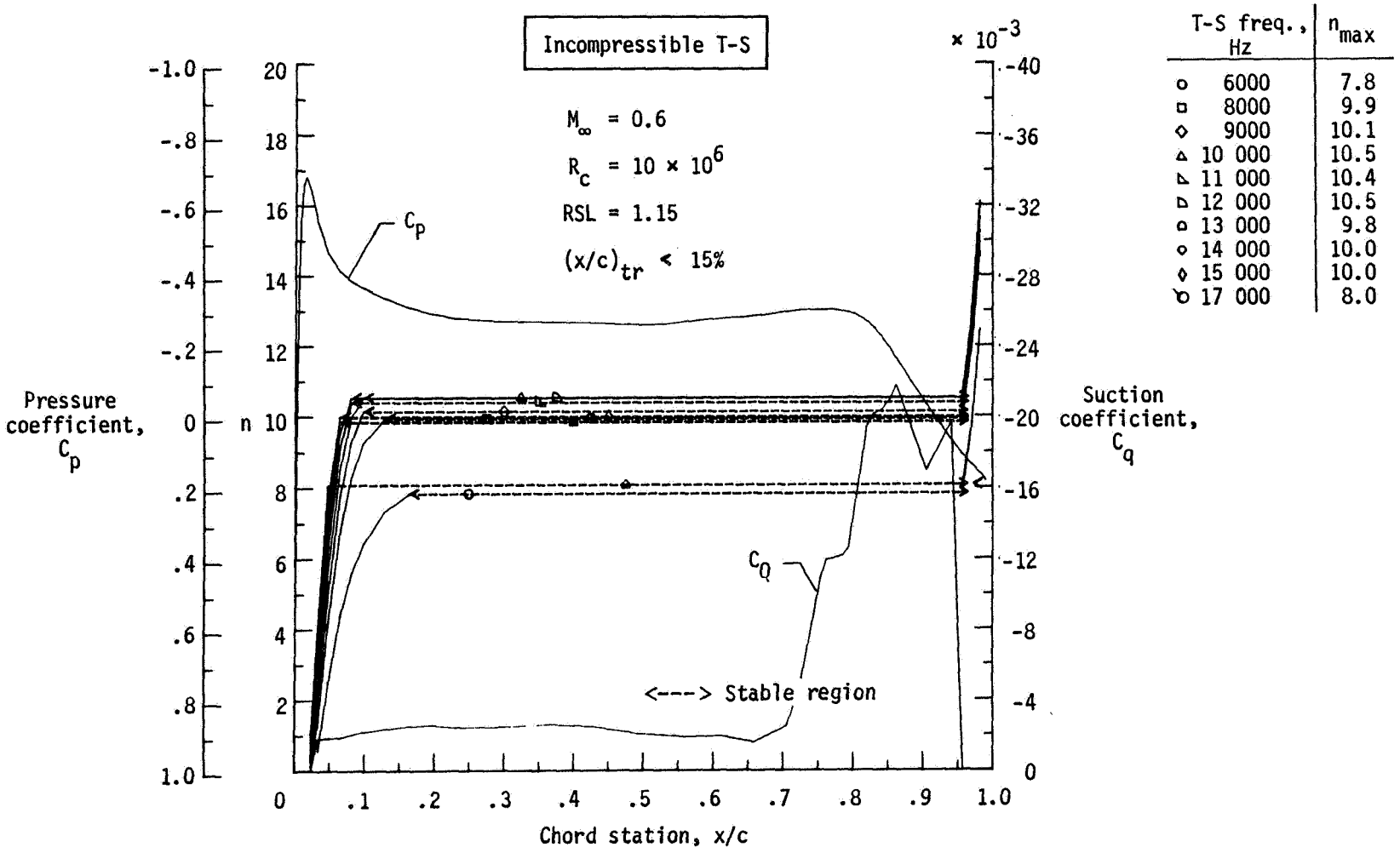

T-S freq., Hz	n_{max}
6000	7.8
8000	9.9
9000	10.1
10 000	10.5
11 000	10.4
12 000	10.5
13 000	9.8
14 000	10.0
15 000	10.0
17 000	8.0

Figure 15(a).- Incompressible TS calculations for case 4, M_∞ = 0.6, R_c = 10 million and RSL = 1.15.

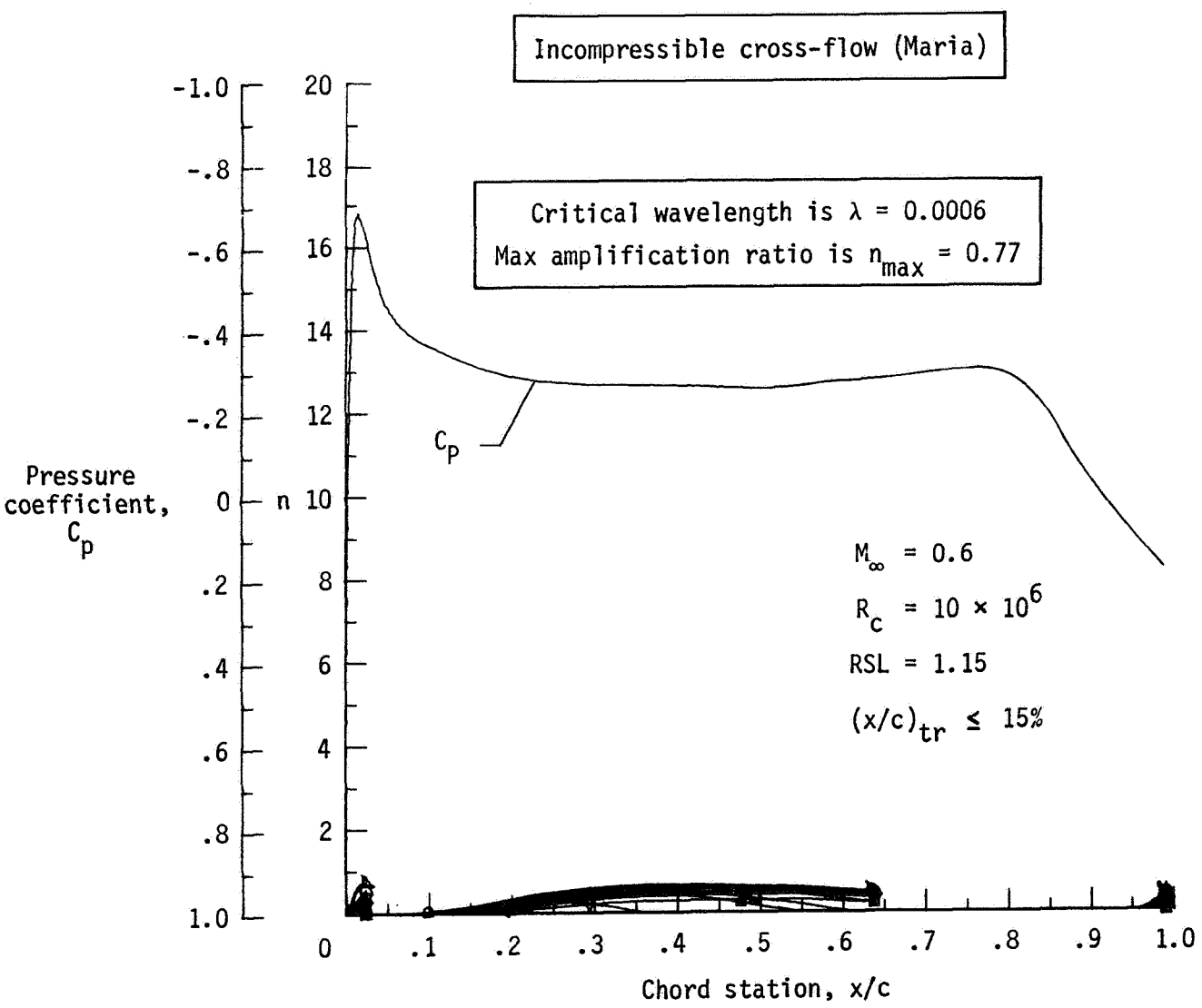

Figure 15(b).- Incompressible CF calculations for case 4, M_∞ = 0.6, R_c = 10 million and RSL = 1.15.

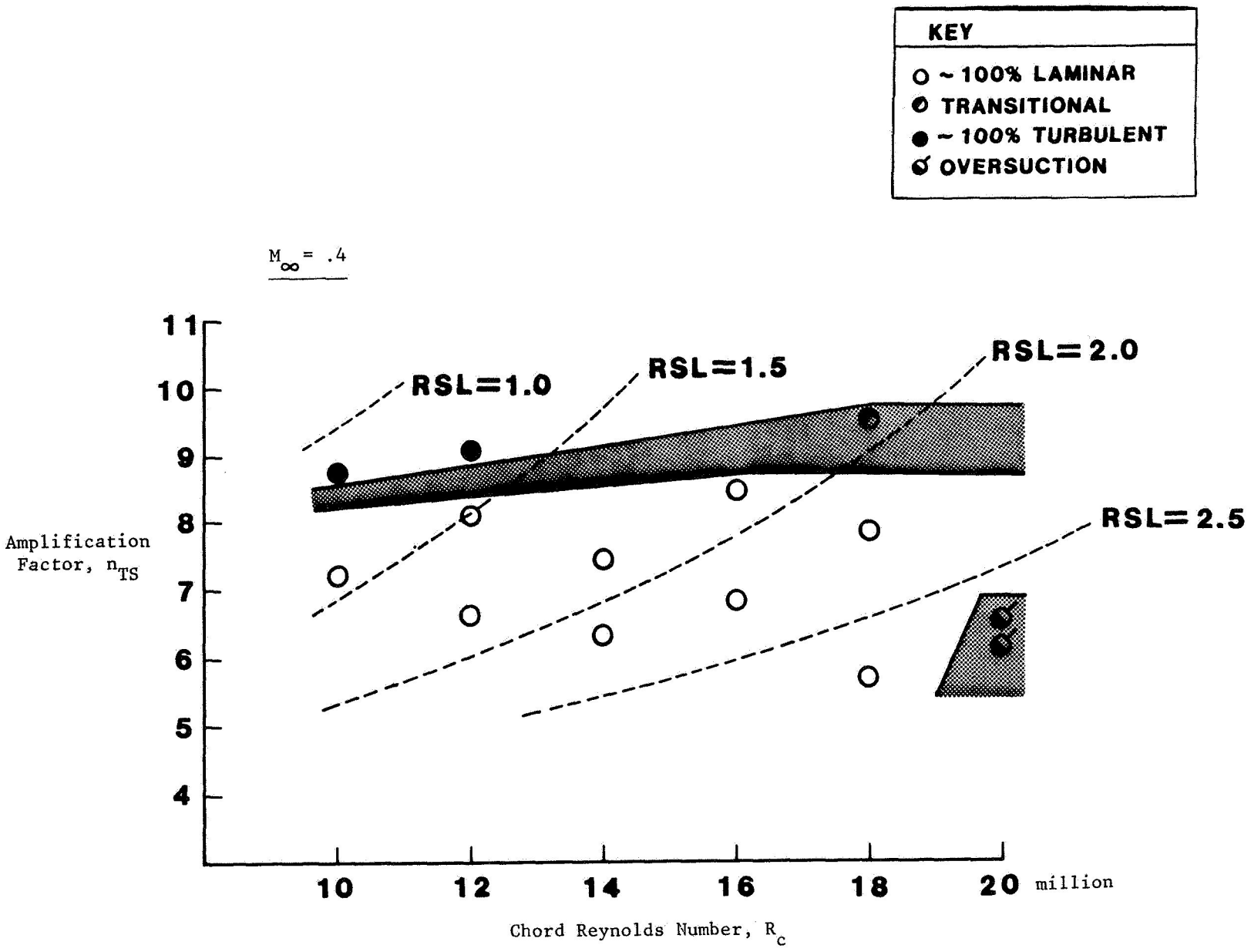

Figure 16.- TS amplfication summary plot for M_∞ = .4.

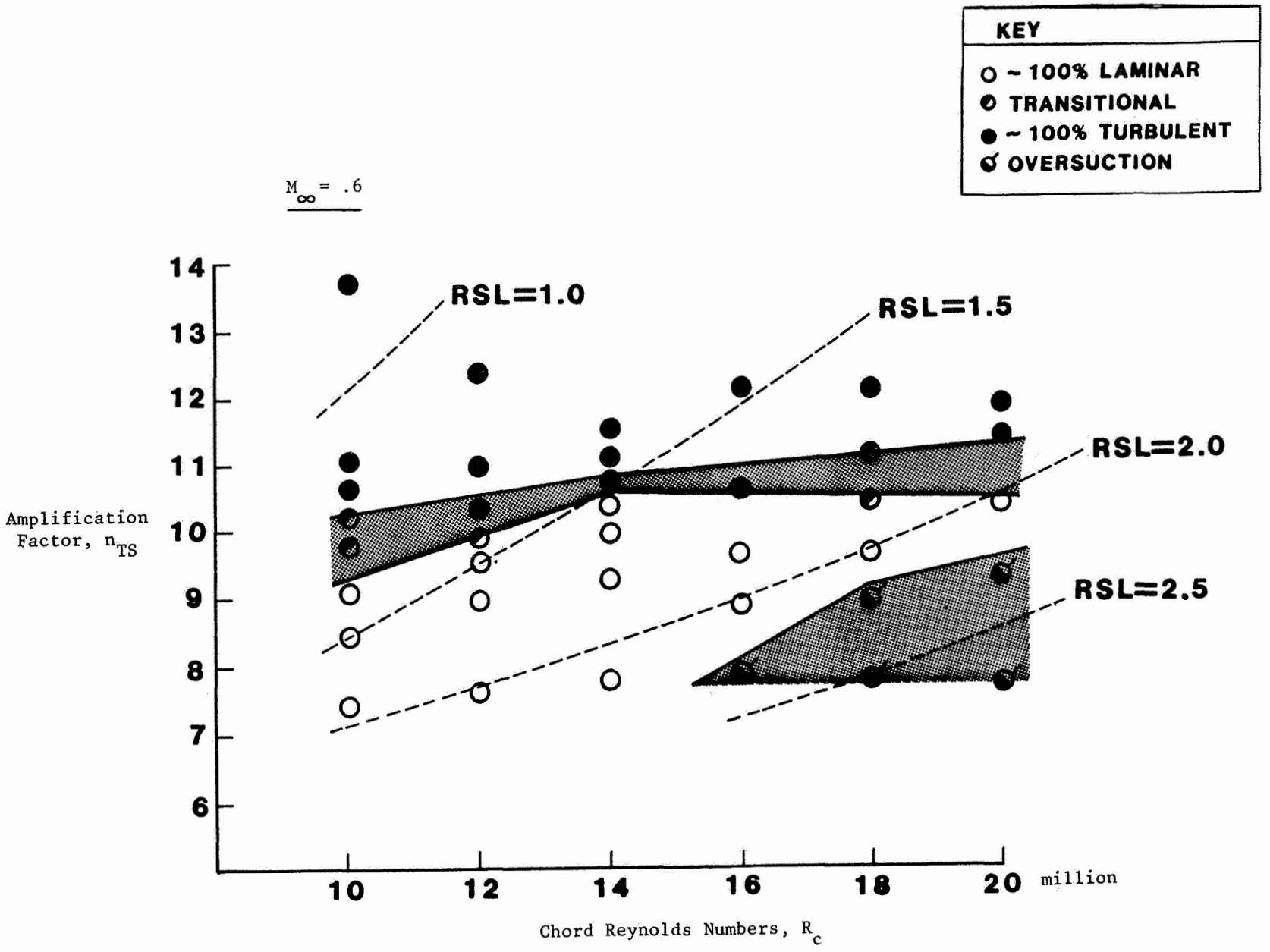

Figure 17.- TS amplification summary plot for M_∞ = .6.

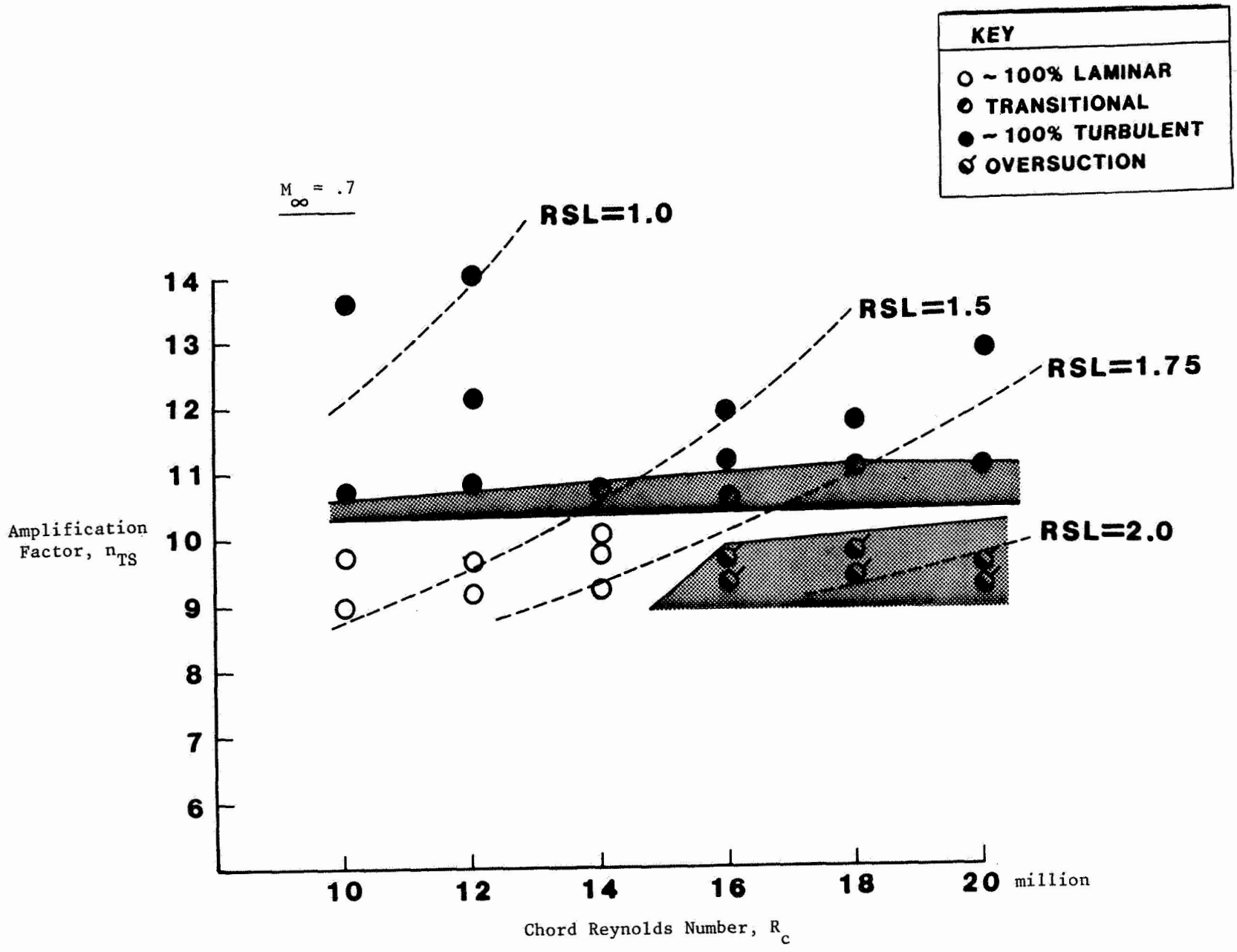

Figure 18.- TS amplification summary plot for M_∞ = .7.

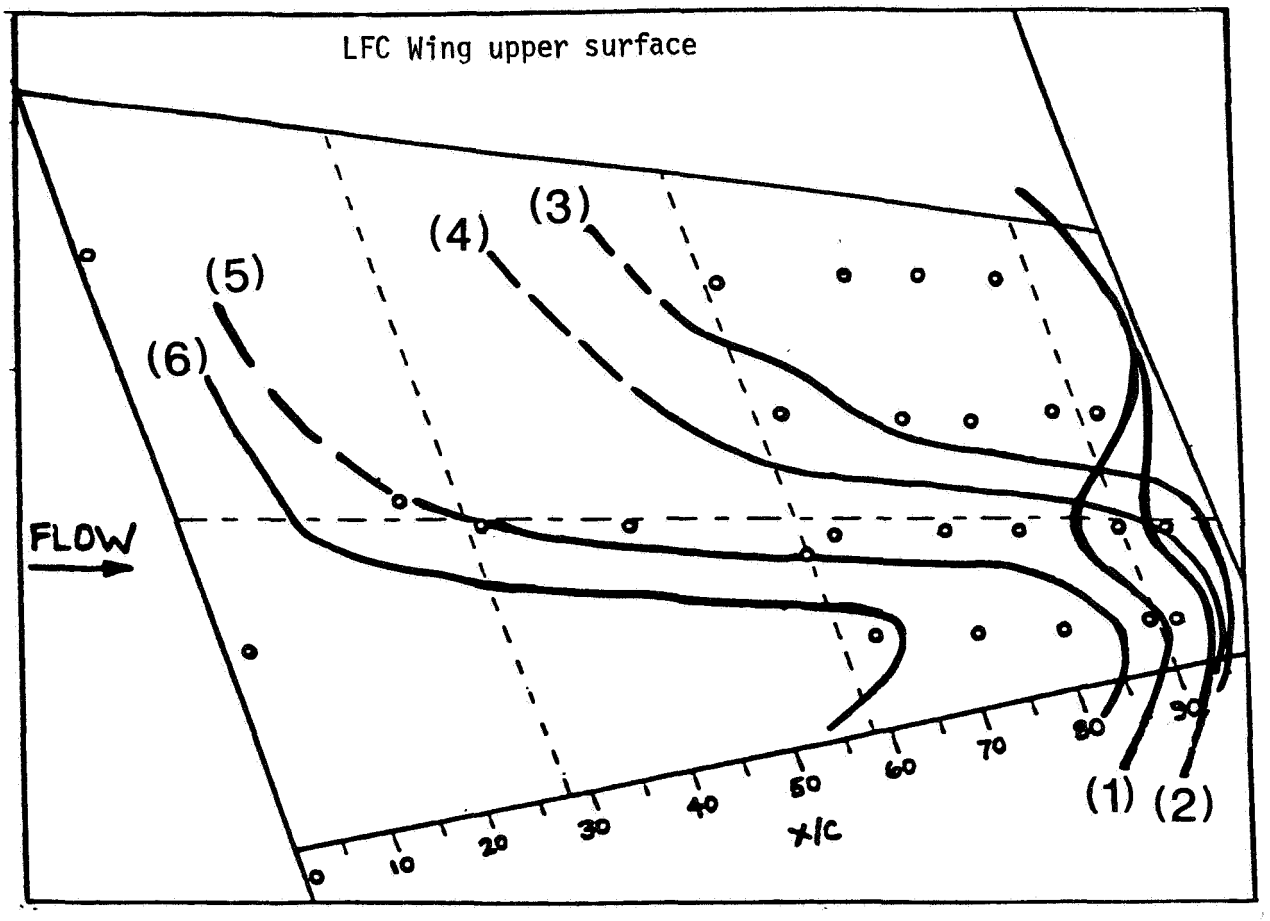

CURVE	RSL	$(X/C)^*_{tr}$	CONDITION
1	2.56	~ 85%	OVERSUCTION
2	2.16	~ 90%	OVERSUCTION
3	2.01	> 95%	LAMINAR
4	1.80	~ 90%	TRANSITION
5	1.72	~ 20%	TRANSITION
6	1.61	< 20%	TURBULENT

* ALONG CENTER-SPAN

Figure 19.- Effect of oversuction on transition.
M_∞ =.6 R_C=18 million

$10 \leqq R_c \leqq 20$ million

$\Lambda = 23^\circ$, upper surface

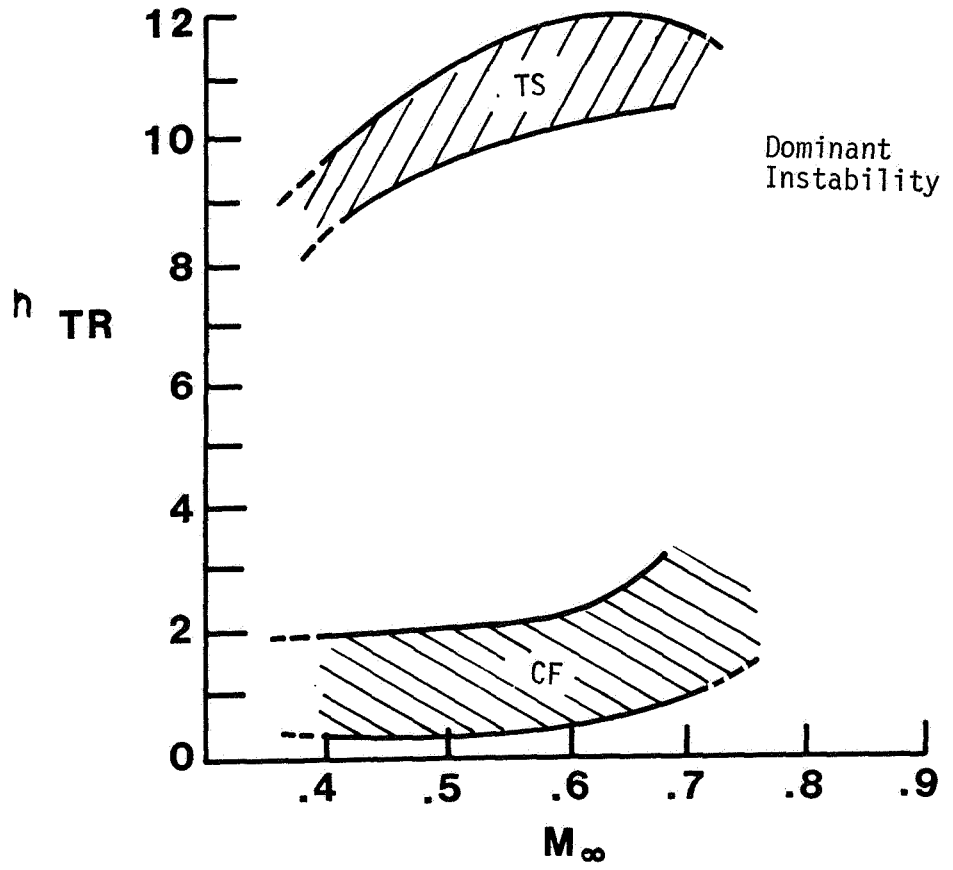

Figure 20.- Calculated incompressible n-factors at transition for swept LFC airfoil.

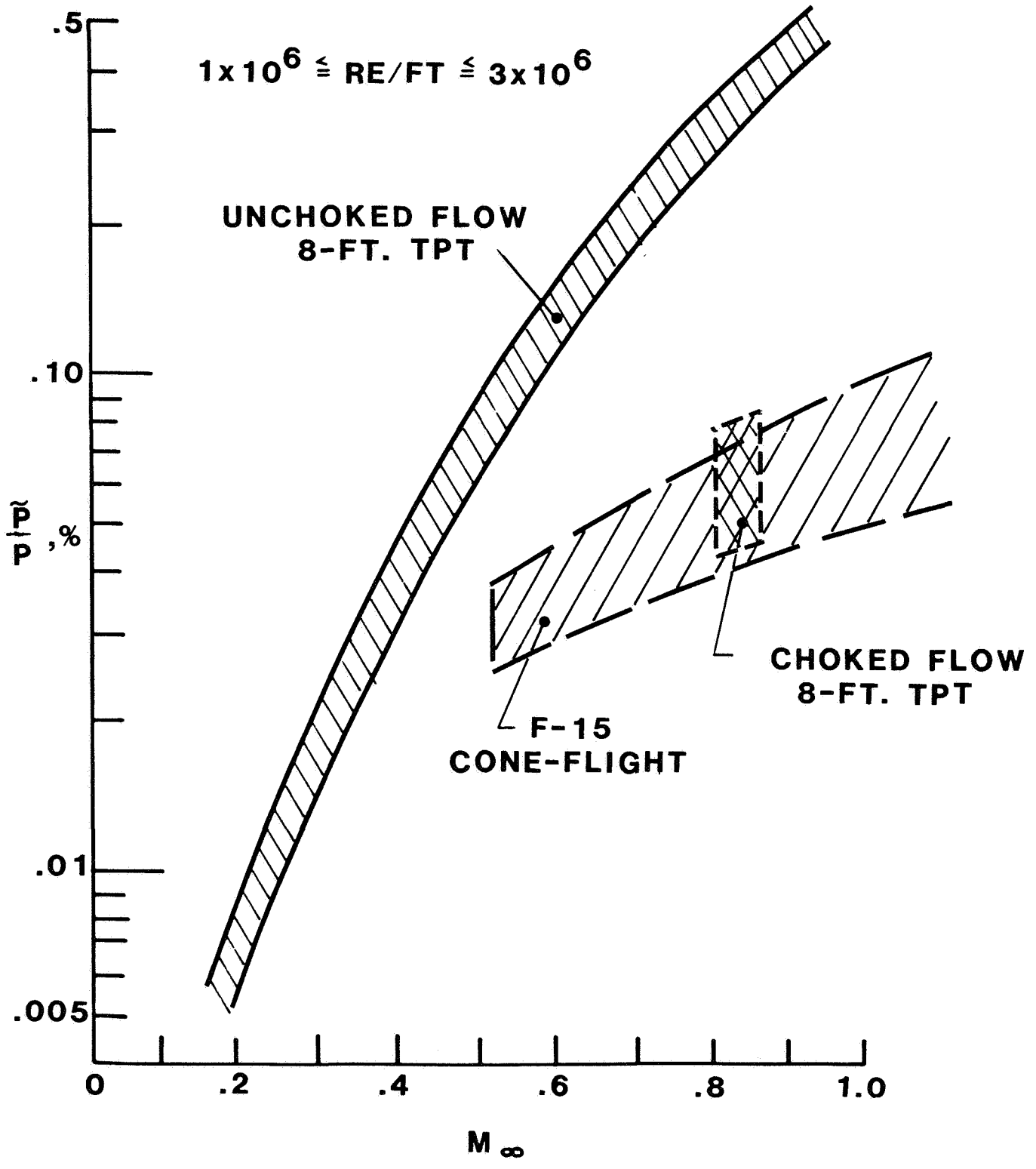

Figure 21.- Measured pressure fluctuations in the 8-Ft. TPT (ref. 27).

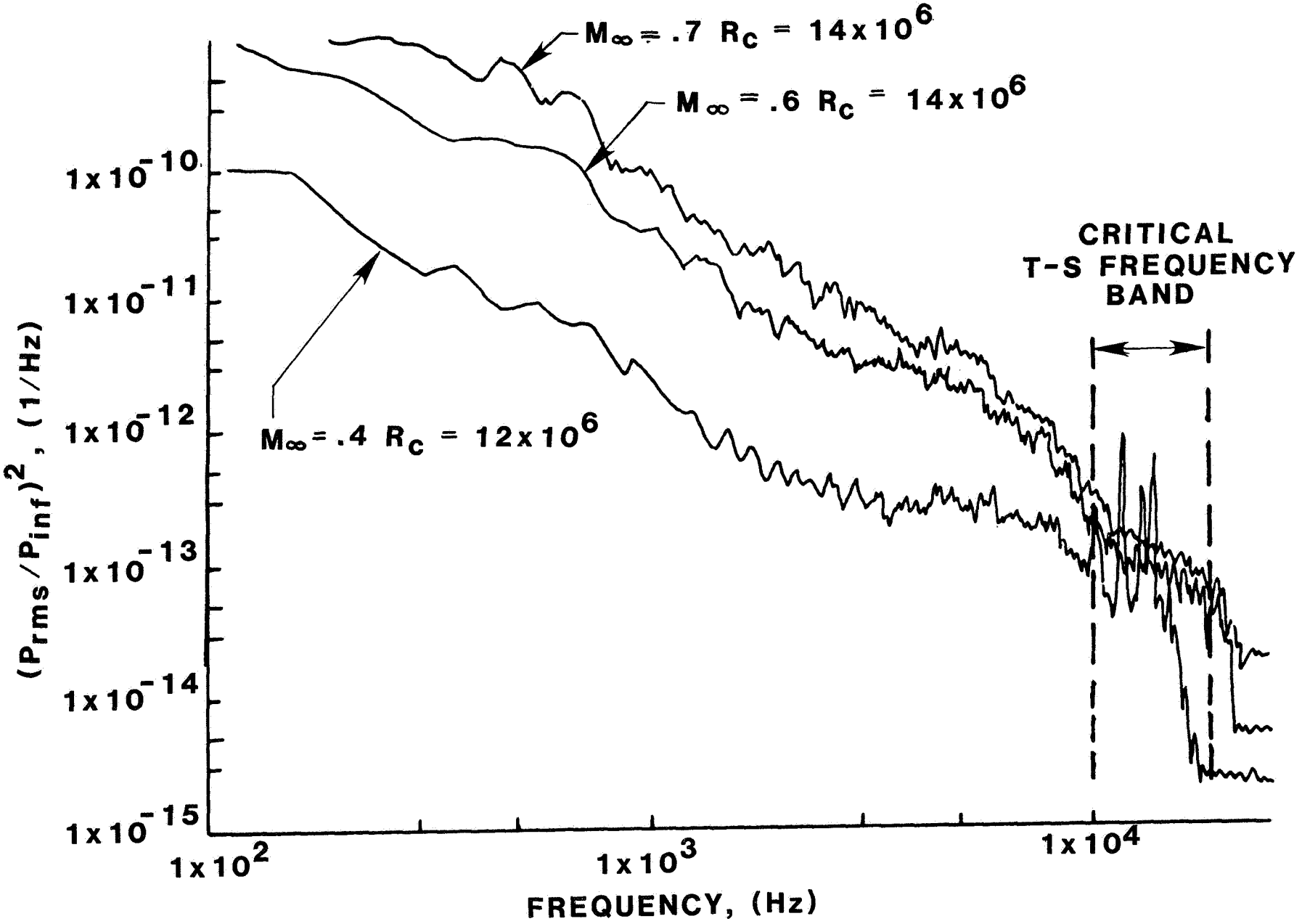

Figure 22.- Sample noise spectra from upstream acoustic transducers.

1. Report No.	2. Government Accession No.	3. Recipient's Catalog No.
NASA CR-3999		

4. Title and Subtitle	5. Report Date
Incompressible Boundary-Layer Stability Analysis of LFC Experimental Data for Sub-Critical Mach Numbers	July 1986
	6. Performing Organization Code
7. Author(s)	8. Performing Organization Report No.
Scott A. Berry	
	10. Work Unit No.
9. Performing Organization Name and Address	
The George Washington University Joint Institute for Advancement of Flight Sciences Langley Research Center Hampton, VA 23665-5225	11. Contract or Grant No. NCC1-24
	13. Type of Report and Period Covered
12. Sponsoring Agency Name and Address	Contractor Report
National Aeronautics and Space Administration Washington, DC 20546-0001	14. Sponsoring Agency Code 505-60-21-01

15. Supplementary Notes

Langley Technical Monitor: J. Ray Dagenhart

The information presented in this report was offered as a dissertation in partial fulfillment of the requirements for the Degree of Master of Science, The George Washington University, Hampton, Virginia, January 1986.

16. Abstract

An incompressible boundary-layer stability analysis of Laminar Flow Control (LFC) experimental data was completed and the results are presented. This analysis was undertaken for three reasons: to study laminar boundary-layer stability on a modern swept LFC airfoil; to calculate incompressible design limits of linear stability theory as applied to a modern airfoil at high subsonic speeds; and to verify the use of linear stability theory as a design tool. The experimental data were taken from the slotted LFC experiment recently completed in the NASA Langley 8-Foot Transonic Pressure Tunnel. Linear stability theory was applied and the results were compared with transition data to arrive at correlated n-factors. Results of the analysis showed that for the configuration and cases studied, Tollmien-Schlichting (TS) amplification was the dominating disturbance influencing transition. For these cases, incompressible linear stability theory correlated with an n-factor for TS waves of approximately 10 at transition. The n-factor method correlated rather consistently to this value despite a number of non-ideal conditions which indicates the method is useful as a design tool for advanced laminar flow airfoils.

17. Key Words (Suggested by Author(s))	18. Distribution Statement
Boundary-Layer Stability Tollmien-Schlichting Instability Laminar Flow Control	Unclassified - Unlimited Subject Category 02

19. Security Classif. (of this report)	20. Security Classif. (of this page)	21. No. of Pages	22. Price
Unclassified	Unclassified	82	A05

For sale by the National Technical Information Service, Springfield, Virginia 22161

NASA-Langley, 1986

National Aeronautics and
Space Administration
Code NIT-4

Washington, D.C.
20546-0001

Official Business
Penalty for Private Use, $300

BULK RATE
POSTAGE & FEES PAID
NASA
Permit No. G-27

NASA

POSTMASTER: If Undeliverable (Section 158 Postal Manual) Do Not Return